A numerical simulation of hybrid nanofluid flow with homogenous-heterogenous reactions over a curved surface

Thesis Submitted By

ABIDA RAFIQ
(01-248181-001)

Supervised By

Prof. Dr. M. Ramzan

A dissertation submitted to the Department of Computer Science, Bahria University, Islamabad as a partial fulfillment of the requirements for the award of the degree of MS (Mathematics)

Session (2018-2020)

Bahria University
Discovering Knowledge

MS-13

Thesis Completion Certificate

Student's Name: **Abida Rafiq** Registration No: **56132** Programme of Study: **MS Mathematics**

Thesis Title: **A Numerical simulation of hybrid nanofluid flow with homogeneous heterogeneous reactions over a curved surface.**

It is to certify that the above student's thesis has been completed to my satisfaction and, to my belief, its standard is appropriate for submission for Evaluation. I have also conducted plagiarism test of this thesis using HEC prescribed software and found similarity index at **17%** that is within the permissible limit set by the HEC for the MS/MPhil degree thesis. I have also found the thesis in a format recognized by the BU for the MS/MPhil thesis.

Principal Supervisor's Signature: _____

Date: 4-2-2020 Name: Prof. Dr. M. Ramazan

Bahria University
Discovering Knowledge

MS-14A

Author's Declaration

I, **Abida Rafiq** hereby state that my PhD thesis titled "**A Numerical simulation of hybrid nanofluid flow with homogeneous heterogeneous reactions over a curved surface**" is my own work and has not been submitted previously by me for taking any degree from this university **Bahria University** or anywhere else in the country/world.

At any time if my statement is found to be incorrect even after my Graduate the university has the right to withdraw/cancel my PhD degree.

Name of student: **Abida Rafiq**

Date: **4-2-2020**

Bahria University
Discovering Knowledge

MS-14B

Plagiarism Undertaking

I, solemnly declare that research work presented in the thesis titled "**A Numerical simulation of hybrid nanofluid flow with homogeneous heterogeneous reactions over a curved surface**" is solely my research work with no significant contribution from any other person. Small contribution/help wherever taken has been duly acknowledged and that complete thesis has been written by me.

I understand the zero tolerance policy of the HEC and Bahria University towards plagiarism. Therefore, I as an Author of the above titled thesis declare that no portion of my thesis has been plagiarized and any material used as reference is properly referred/cited.

I undertake that if I am found guilty of any formal plagiarism in the above titled thesis even after award of PhD degree, the university reserves the right to withdraw/revoke my PhD degree and that HEC and the University has the right to publish my name on the HEC/University website on which names of students are placed who submitted plagiarized thesis.

Student/Author's Sign:

Name of the Student: **Abida Rafiq**

Dedicated to

My beloved Husband
children and Respected Supervisor

Acknowledgments

Words are limited to praise **ALLAH**, the most Gracious and the most Beneficent who bestowed me with the knowledge to think into His secrets. I'm really blessed as He fulfilled my wish of higher studies at this stage of my life.

I would like to express my special thanks to my supervisor Prof. Dr. M. Ramzan, who supported and encouraged me within the whole period of my MS degree.

My intense recognition is to my husband Ishtiaq and brother Yasin, who were always real pillars for my encouragement. I am very grateful to Nomana Abid who supported and guided me at every stage and Nosheen Gul were specially remained enormously helpful throughout the period of my MS studies. Humble prayers, continuing support and encouragement of my family are as highly appreciated.

Abida Rafiq

Bahria University Islamabad, Pakistan

February 4th, 2020

Abstract

This study discusses the flow of hybrid nanofluid, an amalgamation of Nikel-Zinc ferrite and Ethylene glycol, over a curved surface with heat transfer analysis. The heat equation contains nonlinear thermal radiation and heat generation/absorption effects. The envisioned mathematical model is supported by the slip thermal boundary layer and homogenous heterogenous reactions over curved surface. Apposite transformations are betrothed to obtain the system of ordinary differential equations from the governing system in curvilinear coordinates. Numerical solution is found by applying MATLAB build-in function *bvp*4*c* .Graphical illustrations and the numerically computed estimates are discussed and analyzed properly. It is comprehended that velocity and temperature distributions have varied behaviors near and far away from the curve when curvature parameter is enhanced.

TABLE OF CONTENTS

LIST OF TABLES

LIST OF FIGURES

NOMENCLATURE

U, v	Velocity components in the x- and r- direction
r, x	Curvilinear coordinate
R^*	Dimensionless radius of circle
P	Pressure
B_0	Strength of magnetic field
Q_0	Volumetric rate of heat generation/absorption
q_r	Nonlinear radiative heat flux
T, T_∞	Temperature
C, C_w, C_∞	Concentration
D_B	Brownian diffusion coefficient
m^*	Mass
c_p, c	Specific heat
V	Volume
F^*	Force
L^*	Strain tensor
ΔT	Temperature difference between two systems
T_f	Convective temperature at the sheet
L	Value of slip parameter
j_W	Mass flux
u_w	Stretching velocity along x-direction
k^*	Mean absorption coefficient
K_1	Curvature parameter
Ha	Magnetic parameter
s	Positive stretching constant

k_1, k_2	Strength of homogenous-heterogeneous reactions
Sc	Schmidt number
R_d	Radiation parameter
h^*	Convective heat transfer coefficient
K	Slip parameter
k_c, k_s	Rate constant
$\mathrm{Re_x}$	Local Reynolds number
$E_{gen'''}$	Volumetric rate of local entropy generation
E_0	Characteristic entropy generation rate
N_G	Entropy generation
Br	Brinkman number
Nu_x	Nusselt number
C_s	Heat capacity of surface
Sh_x	Sherwood number
D_T	Thermophoretic diffusion coefficient
Bi	Biot number
Pr	Prandtl number
C_f	Surface drag force
A, B	Chemical species
c_1, c_2	Concentration of chemical species
k_c, k_s	Rate constant
Dc_1, Dc_2	Diffusion coefficient
$\frac{D}{Dt}$	Material time derivative
$\frac{du}{dx}$	Gradient of velocity

Greek symbols

Φ	Solid volume fraction of nanofluid

ρ_{nf} , ρ_f , ρ_s	Density
μ_{nf} , μ_f , μ_s	Dynamic viscosity
σ^*	Stefan-Boltzmann constant
ξ	A scaled boundary-layer coordinate
η_1	Apparent viscosity
σ	Electrical conductivity
σ_{nf}	Modified thermal diffusivity
υ	Kinematic viscosity
θ_w	Temperature difference
λ_1	Heat generation parameter
f	Dimensionless stream function,
θ	Dimensionless temperature
τ_{rx}	Wall's shear stress
$\sum$	A constant parameter
α	Dimensionless temperature difference
$\left(\rho C_p\right)_{nf}, (\rho C_p)_f$	Heat capacity

Subscripts

∞	Use for ambient
w	For wall surface
nf	For the nanofluid
f	For the base fluid
P	For the solid (nanoparticles)
x	Partial derivative w.r.t x

Chapter 1

Introduction and literature review

1.1 Introduction

Conventional heat transmission fluids innately have low thermal conductivity as compared to solids. Thermal conductivity of these fluids can be enhanced by adding nanoparticles. The concept of nanofluid was floated by Choi [1] in 1995. Due to anomalous thermal conductivity and improved stability, nanofluids have encouraging future, even for small fractions of suspended nanoparticals as coolants [2-4]. Existing applications of nanofluid based nanotechnology are nano devices, oil refineries, nuclear reactor, automobile industry and cooling procedures of energy conversion. The use of nanoparticles to enhance thermal conductivity of base fluid is main reason to make nanofluid. Base fluids have low thermal conductivity and consist of:

- Water.
- Ethylene-glycols and other coolants.
- Oil and other lubricants.

These fluids have poor capability of heat transfer due to low thermal conductivity. A small amount of nanoparticles ($< 1\%$) is dispersed in base fluid to increase the thermal conductivity of base fluid. The material used for nanoparticles are:

- Oxide ceramics: Al_2O_3,Cuo.
- Metal Carbides: SiC.
- Nitrides: SiN, AIN.
- Metals: Cu, Al.

Thermal conductivity of nanoparticals depends upon size, shape, particle volume fraction, material, temperature and base fluid. For example, nanofluid with non-metallic (oxides) have less thermal conductivity than metallic nanoparticles. Nanofluids have higher thermal conductivity with smaller particle size. Nanofluids with the cylindrical shaped particles show more augmentation in thermal conductivity as compared to the spherical shaped nanoparticles, called nano-tubes or rods [5]. The commonly used nanoparticles by many researchers are Copper oxide (CuO) and Alumina (Al_2O_3).

Presently, sustainable energy generation is one of the biggest challenge faced by the societies. The solution of this issue is solar energy which is a natural source to get heat and electricity. Thermal radiation transformed by solar energy has notable influence in many engineering applications such as advanced power plants, gas turbines, gas cooled atomic (nuclear) reactor, hypersonic flight and aeronauts. Heat transfer is controlled by radiative effects in polymer processing industry. In last few years many researchers have discoursed convection of heat transfer and their application. More than one type composite nanostructures can be added in a base fluid to enhance the performance of nanofluid known as hybrid nanofluid. Numerical studies and experiments regarding hybrid nanofluid are still being done [6-9]. It is noticed that the thermo-physical properties of the fluid with hybrid nanoparticles and concluded the remarkable thermal efficiency. Abbasi et al. [10] used hybridization of carbon nanotubes and alumina. They noticed thermal conduction and the stability. Next generation heat transfer liquids are hybrid nanofluids because they provide stimulating new options to increase heat transmission efficiency as compared to nanofluid. Material used for hybrid nanofluids are:

- Metal matrix nanocomposites (MMNC): Al_2O_3/Ni, MgO/Fe, Al/CNT, Mg/CNT, Al_2O_3/Fe-Cr, Al_2O_3/Cu.
- Ceramic matrix nano-composites (CMNC): Al_2O_3/SiO_2, Al_2O_3/SiC, Al_2O_3/Carbon nano-tubes, Al_2O_3/Cu.
- Polymer matrix nanocomposites (PMNC): polyester/TiO_2, polymer/ (LDHs) layer double hydroxide, polymer/Carbon nano tubes (CNT).

For all cases, size of the hybrid (nanocomposites) particle should be < 100 nm. Base fluids of hybrid nanofluids are:

- Water.
- Oil.
- Etylene glycol.

Most of the researchers used water and etylene glycol both as a base fluid (hybrid nanofluids) [11-13]. Very few research work of oil-based hybrid nanoluids have been found [14-15]. They found that oil-based hybrid nanofluids have better result than water based hybrid nanofluid. Hybrid nanofluids have vast use in the application of heat transfer such as refrigeration, automobile radiators, generator cooling, electronic cooling, welding, thermal storage, nuclear system cooling, lubrication, defence, biomedical, drug reduction, coolant in machining, gas turbine, solar heating, cooling and heating in buildings and other industrial area.

Homogeneous-heterogenous reactions are involved in several processes of heat transfer and commercial eminence like catalytic oxidation, combustion and biochemical system. Chemical reaction can be classified as homogeneous or heterogenous reaction depending upon they take place constantly through a given phase or occur on other phase respectively. The heterogenous reactions occur on some surfaces of catalytic while homogeneous reactions occur in the large quantity of the fluid. This interaction is used in

the destruction and production of reactive species at various levels on fluid and catalytic surfaces. Researchers and scientists are intended to design and construct a new catalytic processes which work at maximum heat(temperature).

1.2 Literature Review

In the previous years, researchers have faced an important challenge of thermal efficiency in different industrial and engineering applications. Technology has made huge advancements in the field of transportation, high speed microelectronics, chemical synthesis, micro systems inclusive of electro-mechanical components high thermal loads carrier. The main concern now-a-days is cooling of these equipments. Customarily, the rate of heat transmission is increased due to increasing the available heat exchange area. A different way is to disperse the nano-sized structures within the fluids having less thermal properties (conventional heat transmission fluids), like water, ethylene glycol, propylene glycol, etc. [16]. Choi [1] was pioneer of enhancing the thermal properties of these liquids, called 'nanofluid'. This revelation further enter the researchers into a new research era. Numerous scientists adopted this idea and hence, a few resulting models have been effectively proposed. A model to analyze the thermal conductivity effectiveness of nanofluids was proposed by Maxwell [17]. This model includes the spherical addition of nanoparticles and the thermal conductivity of base fluid and nanoparticles. Hamilton and Crosser [18] suggested a model which overcome this deficiency, it is suitable for non-spherical shaped nanoparticles. The researchers introduced many models in this area which investigated the effects of types, size and shapes of nanoparticles [19–24].

Despite the fact that nanofluids have alot of capability to meet the developing thirst of thermal efficiency, still researchers are enthusiastically searching different types of fluids. The advanced type of nanofluids are hybrid nanofluids which show an impressive thermal efficiency as compared to nanofluids. Two or more different types of smaller particles dispersed in the base fluid or composite nanostructure in to the base fluid is called

hybrid nanofluids. This gives a homogeneous mixture having physico-chemical properties of different substances which can barely be envisioned to exist in a single substance [25]. In several heat transfer applications such as automobiles, electronics, industry and biomedical usage of hybrid nanofluid can be noticed. Due to positive features of hybrid nanofluids like chemical stability and high thermal efficiency play a significant role in the industry as compared to nanofluids.

Generally used nanoparticles are metals, metal oxides, metal nitrides, metal carbides carbon nanotubes, graphite, diamond (carbon materials). Pak and Cho [26] observed heat transmission enhancement of water with TiO_2 or Al_2O_3 nanofluids. Xuan and Li [27] used Copper in water and Copper/transformer oil nanofluids and noticed the increase in heat transmission than the base fluids. Nine et al. [28] examined thermal characteristics of Al_2O_3-MWNTs (Alumina multi-walled carbon nanotubes)/water hybrid nanofluids. Baghbanzadeh et al. [29] investigated silicon MWCNTs (multi-walled carbon nanotubes) and Munkhbayar et al. [30] discussed the silver MWCNTs (multi-walled carbon nanotubes). Further carbon nanotubes (CNTs) reported by Jana et al. [31]. Multi-walled carbon nano-tubes (MWCNTs-Fe_2O_3/water nanofluids) are investigated by Sundar et al. [32-34]. Use of nikle-zinc ferrite can be noticed in number of electro-magnetic applications with high permeability, e.g., inductors and electro-magnetic wave absorber. Several researchers [35-37] recommended the use of nickel-zinc ferrite, in order to reduce energy destruction related to bulk powders. Furthermore, many electronic appliances need such material with required thickness and compressed into outsized shapes. To get nickel-zinc ferrite various methods have been recommended, which are hydrothermal, ball milling and precipitation. Ferrofluids are colloidal fluids consist of suspended ferro-magnetic or ferri-magnetic nanoparticles in an electrically insulated carrier fluid. In the ongoing examination ($C_2H_6O_2$) ethylene glycol was taken as a carrier fluid. The normal spinal structure of crystallize nickel–zinc ferrite ($NiZnFe_2O_4$) was assumed as a nanoparticle. At room temperature the inverted spinals are ferro-magnetic and normal spinals are para-magnetic. Zinc-ferrites act like antiferro-magnetic in nature at low temperature.

This phenomena ferro-magnetic nanofluid is more suitable in different application of real world [38-39]. Neuringer [40] discussed the effects of the magnetic field and thermal gradient of ferro-fluid flow. The heat transmit investigation in a ferro-magnetic fluid flow is demonstrated by Majeed et al. [41].

The fluid flow over a stretched surface has many applications in industrial processes and engineering, liquid films in condensation process, paper production, drawing of plastic wires and films, crystal glowing, glass blowing, food industries, coatings, drug delivery system, paints, ceramics, manufacturing of rubber sheets,etc. Flow produced by stretching sheet is discussed by Crane [42]. Many researchers examined stretching flow under different configurations but the remarkable work done by Gupta and Gupta [43] who exaimned the flow over spongy surface. Hydromagnetic flow past a stretching surface is assumed by Charabakti and Gupta [44]. Anderson et al. [45] exaimned the Power-law fluid flow under the effect of magnetic forces over a linearly stretched surface. An Oldyroyd-B fluid flow with the influence of generation/absorption is depicted by Hayat et al. [46]. Fluid flow over curved stretching surface using curvilinear coordinate was first investigated by Sajid et al. [47]. The impact of thermal stratification in the ferromagnetic fluid past a stretching sheet is investigated by Muhammad et al. [48]. Ramzan and Yousaf [49] determined that the elastic viscous nanofluid in view of Newtonian heating, over a two dimensional stretchig sheet. Sanni et al. [50] obtained a numerical solution for the viscous fluid flow over a stretched curved surface. Hussain et al. [51] applied the exponentially stretching surface by analyzing the flow of Jeffery nano fluid along with radiation effects. Some recent researches work on various fluid flows over stretched surface with coating can be found in references [52-55].

Homogeneous and heterogenous reactions are involved in many bio chemical reacting system for example bio-chemical systems, oxidization and catalysis. The association of homogenous and heterogenous reactions is very complex. Some of the reactions have ability to continue gradually or no more except in the presence of a catalyst. Homogenous and heterogenous reactions are unpredictable involving production and consumption of

reactant species both within the fluid and on the catalyst surface at different rates. Such reactions involve in fog formation, processing and dispersion of food, polymer's production, hydro-metallurgical industry and ceramics. Homogenous-heterogenous (HH) reactions for the viscous fluid past a flat surface is investigated by Merkin [56]. He inspected heterogenous reaction on the catalyst surface and homogenous reaction for cubic autocatalysis. The surface reaction is effective near the surface. Chaudhary and Markin [57] reported the homogenous-heterogenous reactions with equal diffusivities. Bachok et al [58] determined the homogenous heterogenous reactions in stretched flow. Stretched flow of viscous fluid with homogenous heterogenous reactions is assumed by Khan and Pop [59]. Homogenous heterogenous reactions can be consulted through the investigations [60-62] and various studies therein.

From the above literature review, it is noted that very less research work is available on curved surface as compared to linear/non-linear/exponential stretching surface. And, further this difference gets narrower by coming towards the study of hybrid nanofluid with homogenous heterogenous reactions past curved surfaces. For this purpose, our focal point of this whole debate is to discuss hybrid nanofluid flow comprising ferro-magnetic nanoparticlesi.e., nickel-zinc ferrite ($NiZnFe_2O_4$) and the base fluid of base, ethylene glycol($C_2H_6O_2$) over a curved surface with homogenous heterogenous reactions. All the numerical solutions are obtained using *bvp4c* from MATLAB, and all the characteristics of study parameters are discussed thoroughly by keeping their physical justification in mind.

Chapter 2

Preliminaries

This chapter contains standard definitions and fundamental equations which are supportive in understanding the work in the third and fourth chapters.

2.1 Fluid

Any substace that flows or continuously deforms subjected to a shear stress. Examples of fluid are paints, shampoos, cooking oil, blood and oxygen etc.

2.1.1 Liquid

Fluid that has definite volume but no definite shape. Examples are water, milk, blood etc.

2.1.2 Gas

It is type of fluid which has no definite shape and volume. Examples are Oxygen, Nitrogen, Hydrogen etc.

2.2 Fluid mechanics

Fluid mechanics is the examination of the behavior of liquids at rest or in motion. It can be classified into two subclasses.

2.2.1 Fluid statics

Fluid mechanics is the study of behavior of liquids at rest.

2.2.2 Fluid dynamics

Examination and investigation of the flow of fluid is called fluid dynamics.

2.3 Stress

Force applied per unit area within the deformable body is called stress. Unit of stress in SI is Nm^{-2} or kg/m^2 and $[M/LT^2]$ is its dimension. Stress is divided in to two types.

2.3.1 Shear stress

When the acting force is parallel to the unit area of the surface then it is called shear stress.

2.3.2 Normal stress

The force act normaly or perpendicularly per unit area of the surface is recognized as normal stress.

2.4 Strain

A quantity which measure destortion(deformation) of an object when a force acts on it.

2.5 Flow

Flow is distinguished as a material that deforms smoothly and steadily under the effects of different kinds of forces. Flow is divided into two major subclasses.

2.5.1 Laminar flow

Laminar is a systematic flow, in which fluid flow in regular and well arranged paths, with no intermixing between the layers.

2.5.2 Turbulent flow

Turbulent flow is obtained when the liquid particles moves randomly and have irregular velocity in the flow field.

2.6 Viscosity

It measures the liquid resistance to flow when many forces are acting on it. Mathematically, can be represented as follows:

$$\text{viscosity} = \frac{\text{shear stress}}{\text{Rate of shear strain}}, \tag{2.1}$$

$$\mu = \frac{\tau_{yx}}{(du/dy)}. \tag{2.2}$$

2.6.1 Dynamic viscosity

The measure of fluid resistivity to flow is known as dynamic/absolute viscosity. Its unit is $kg/m.\sec$.

2.6.2 Kinematic viscosity

Kinametic viscosity is the relation of the dynamic viscosity and fluid density. Mathematically, it is shown as:

$$\nu^* = \frac{\text{absolute viscosity}}{\text{fluid's density}}, \tag{2.3}$$

$$\nu^* = \frac{\mu}{\rho}. \tag{2.4}$$

SI unit is $\frac{m^2}{s}$.

2.7 Newtonian fluids

In these fluids the velocity gradient is linearly proportional to shear stress. Kerosene, glycerine, water and ethyl alcohol are some examples of Newtonian fluids.

2.8 Non-Newtonian fluids

Fluids which do not hold the Newton's law of viscosity. There is direct and nonlinear relationship between shear force and gradient of velocity. Soup, butter, cosmetics and lava are the examples of these fluids. Mathematically, represented as follows:

$$\boldsymbol{\tau}_{yx} \propto \left(\frac{du}{dy}\right)^n, \ n \neq 1, \tag{2.5}$$

or

$$\boldsymbol{\tau}_{yx} = \eta \frac{du}{dy}, \ \eta = s\left(\frac{du}{dy}\right)^{n-1}, \tag{2.6}$$

where n is the flow behavior index. For $n = 1$, Eq. (2.6) represents the Newton's law of viscosity. The three major types of non-Newtonian fluids are, (i) differential type (ii) integral type (iii) rate type.

2.8.1 Rate type fluid

Fluids which show the behavior of retardation and relaxation times are rate type fluids. In this type stress is given implicitly in terms of velocity gradient and its higher derivatives. Jeffery, Oldroyd and Maxwell are the examples of rate type fluid models.

2.8.2 Retardation Time

It is the time required to balance an opposing force which is produced when shear stress acts.

2.8.3 Relaxation Time

With the applied stress, the system transform from equilibrium position goes to perturb position. When the stress is taken off, the time needed for a perturbed system back to equilibrium position is known as relaxation time

2.9 Magnetohydrodynamics (MHD)

It is the combination of three words magneto, hydro and dynamic which mean magnetic, water/liquid and motion of object by force respectively. Magnetohydrodynamics is the study of magnetic properties and characterstics of the high conducting fluids. Liquid metals and salt water are some examples of MHD fluids. Its parametric form is called Hartmann number.

2.10 Newton's law of viscosity

Fluids that show the linear and direct relation between velocity gradient and shear stress. Mathematically, it can be shown as follows:

$$\tau_{yx} \propto (du/dy), \tag{2.7}$$

or

$$\tau_{yx} = \mu \left(du/dy \right). \tag{2.8}$$

2.11 Density

Mass of a material per unit volume is called density. It is used to calculate the amount of a material present in a unit volume. Mathematically

$$\rho = \frac{m^*}{V}. \tag{2.9}$$

In SI its unit is kg/m^3.

2.12 Pressure

Pressure is the magnitude of the perpendicularly applied force per unit area. Mathematically, given by:

$$P = (F^*/A). \tag{2.10}$$

Unit of pressure in SI system is N/m^2.

2.13 Homogenous reactions

When the catalyst and reactant both are in same phase during a chemical reaction then it is called homogenous reaction.

2.14 Heterogenous reactions

The reactions in which catalyst and reactant are in two or more phases is known as heterogenous reactions.

2.15 Catalyst

Any material which do not participate in reaction. It only increase or decrease the rate of reaction.

2.16 Reactant

A substance that takes part in and undergoes a change during a chemical reaction.

2.17 Modes of heat transfer

Heat is the form of energy that moves from hotter region to colder. Flow of heat takes place between two objects with different temperatures. The transfer of heat occurs through any one of the following three modes:

2.17.1 Conduction

Flow of heat from warmer to cooler areas in liquids and solids by direct contact of the free electrons and molecules is called conduction. In this process molecules do not move and heat transfers by free electrons. Mathematically

$$\frac{\boldsymbol{q}}{A} = \mathbf{k}\left(\frac{T_2 - T_1}{X_2 - X_1}\right) = \mathbf{k}\frac{\Delta T}{\Delta X}, \tag{2.11}$$

where

$$\boldsymbol{q} = -\mathbf{k}A\frac{dT}{dx}. \tag{2.12}$$

2.17.2 Radiation

Radiation is a process through electromagnetic waves from hotter to colder region without any medium. Mathematically, it is represented as

$$q = e\sigma^* A \left(\Delta T\right)^4 . \tag{2.13}$$

2.17.3 Convection

A mode where heat flows by the movement of molecules from hot to cold area of liquids or gases. Mathematically,

$$q = h^* A \left(T_s - T_\infty\right) . \tag{2.14}$$

2.18 Convective boundary conditions

Convective boundary conditions are also called Robin boundary conditions. These kind of conditions are usually define on boundary (surfaces). Mathematically,

$$\mathbf{k} \left(\frac{\partial T}{\partial m_i}\right)_{x_i} = h^* \left(T_f(x_i, t) - T_w(x_i, t)\right) , \tag{2.15}$$

2.19 Nanofluid

Nanofluid is the combination of liquid and very small particles (called nanometer particles). These fluids are mixture of suspended nanoparticles in the base liquid. Oxides, metals and carbon nanotubes are used to made the nanoparticles. The base fluids are water and oil.

2.20 Hybrid nanofluid

The mixture of two or more different types of nanoparticles distributed within base fluid is known as Hybrid nanofluid.

2.21 Magnetic field

A vector field which defines the magnetic impact of magnetized materials and electrical currents.

2.22 Stefan-Boltzmann constant

Stefan-Boltzmann constant is the constant of proportionality in the Stefan-Boltzmann law: in unit time the total intensity radiated per unit surface area of a black body is proportional to the fourth power of thermo-dynamic temperature. It is represented by the Greek letter σ^*.

2.23 Electrical conductivity

The material ability to carry electric current is called electrical conductivity. Electrical conductivity is also known as specific conductance. It is represented by Greek letter σ.

2.24 Specific heat

Specific heat is the amount of heat per unit mass required to increase the temperature by one degree. The relation between heat change and temperature is expressed as:

$$Q = cm^* \Delta T. \tag{2.16}$$

2.25 Ambient temperature

Air temperature of an object or environment is called ambient temperature.

2.26 Non-dimensional numbers

2.26.1 Reynolds number (Re)

This dimensionless number determine the flow whether it is laminar or turbulent. It is the relation of inertial and viscous forces. Mathematically, it is expressed as:

$$\begin{aligned} \mathrm{Re} &= \text{inertial forces / viscousforces}, && (2.17) \\ &= \frac{U \times L}{\nu^*}, && (2.18) \end{aligned}$$

Less Reynolds number (<2000) describe laminar flow and greater number (>4000) for turbulent flow.

2.26.2 Prandtl number (Pr)

Prandtl number is the ratio of momentum diffusivity to thermal diffusivity. Mathematically, it is expressed as:

$$\begin{aligned} \mathrm{Pr} &= \frac{\nu_f}{\alpha_f^*}, && (2.19) \\ &= \frac{\mu c_p}{k}. && (2.20) \end{aligned}$$

2.26.3 Radiation parameter (R_d)

It defines the relative effect of conduction to the thermal radiation transfer. Mathematically, expressed as:

$$R_d = \frac{16\sigma^* T_\infty^3}{3k^*\mathbf{k}}, \qquad (2.21)$$

2.26.4 Skin drag force coefficient (C_f)

When fluid is flowing over a sheet emerges certain amount of drag that is known as Skin friction coefficient. It takes place between the fluid flow and the solid surface that reduce the rate of flow of fluid. Mathematical expression for Skin friction coefficient is,

$$C_f = \frac{\tau_{rx}}{\frac{1}{2}\rho u_w^2}. \tag{2.22}$$

2.26.5 Nusselt number (Nu_x)

This dimensionless number describes the relation between convection and conduction heat transfer coefficients at the boundary is called Nusselt number. Mathematically,

$$Nu_x = \frac{xq_w}{k_f(T_f - T_\infty)}, \tag{2.23}$$

$$q_w = (q_r)_w - (\frac{\partial T}{\partial r}). \tag{2.24}$$

2.26.6 Biot number (γ)

The ratio between the internal diffusion resistivity and external convection resistance is named as Biot number. Mathematically, it is expressed as:

$$Bi = \frac{h^* \sqrt{\frac{v_f}{s}}}{k_f}. \tag{2.25}$$

2.26.7 Brinkman number(B_r)

The Brinkman number is a dimensionless number associated to heat produced from a wall to a flowing viscous fluid.

$$B_r = \frac{\mu_{nf} u_w^2}{k_{nf} T_f}. \tag{2.26}$$

2.26.8 Schmidt number (Sc)

This dimensionless number is explained as the ratio of non-Newtonian viscosity (kinematic) to mass diffusivity. Mathematically,

$$Sc = \frac{\nu_f}{D_B}, \tag{2.27}$$

2.26.9 Hartmann number(Ha)

The relation of electro-magnetic force to the viscous force is Hartmann number. Mathematically expressed as:

$$Ha = \frac{\sigma B_0^2}{s\rho_f}. \tag{2.28}$$

2.26.10 Chemical reaction parameter (δ)

The non-dimensional number utilized to measure the strength of chemical reaction rate is called chemical reaction parameter and can be written as:

$$\delta = \frac{Dc_2}{Dc_1}. \tag{2.29}$$

2.27 Conservation laws

A measurable quantity that remains unchanged with the progression of time in an isolated system is called conserved quantity and the law which deals with this quantity is recognized as conservation law. The conservation laws that are used for the flow specification in the subsequently analysis are given below,

2.27.1 Mass conservation law

Conservation law for mass defines that the whole mass in any closed system will remain conserved. Mathematically,

$$\frac{D\rho}{Dt} + \rho\boldsymbol{\nabla}.\mathbf{V} = 0, \tag{2.30}$$

or

$$\frac{\partial\rho}{\partial t} + (\rho\boldsymbol{\nabla}.\mathbf{V}) + (\mathbf{V}.\boldsymbol{\nabla})\,\rho = 0, \tag{2.31}$$

or

$$\boldsymbol{\nabla}.\,(\rho\mathbf{V}) + \frac{\partial\rho}{\partial t} = 0. \tag{2.32}$$

The above equation is continuity equation. For the steady flow Eq. (2.31) becomes

$$\boldsymbol{\nabla}.\,(\rho\mathbf{V}) = 0, \tag{2.33}$$

For incompressible fluid, Eq. (2.32) will be stated as:

$$(\boldsymbol{\nabla}.\mathbf{V}) = 0. \tag{2.34}$$

2.27.2 Law of conservation of momentum

It is defined as the total linear momentum of a closed system remains constant. Generally, it is given by:

$$\rho(D\mathbf{V}/Dt) = \operatorname{div}\boldsymbol{\tau}_1 + \rho\mathbf{b}, \tag{2.35}$$

here $\boldsymbol{\tau}_1 = -pI + S$ is the Cauchy stress tensor.

2.27.3 Law of energy conservation

This law is also known as energy equation and is described as total energy is conserved throughout the whole system. For nanofluids, it is specified by:

$$\rho_f c_f \frac{DT}{Dt} = \tau^*.L^* + k\nabla^2 T + \rho_p c_p \left(D_B \nabla C.\nabla T + \frac{DT}{T_\infty} \nabla T.\nabla T \right). \tag{2.36}$$

2.27.4 Law of concentration conservation

For nanoparticles, equation of the volume fraction is

$$\mathbf{V}.\boldsymbol{\nabla}\mathbf{C} + \frac{\partial C}{\partial t} = -\frac{1}{\rho_p}\boldsymbol{\nabla}.\mathbf{j}_p, \tag{2.37}$$

$$\mathbf{j}_p = -[\rho_p D_B \nabla C + \rho_p D_T \frac{\nabla T}{T_\infty}] \tag{2.38}$$

Eq. (2.37) gives after writing value of $\mathbf{j}_p$.

$$\mathbf{V}.\boldsymbol{\nabla}\mathbf{C} + \frac{\partial C}{\partial t} = \mathbf{D_T}\frac{\boldsymbol{\nabla}^\mathbf{2}\mathbf{T}}{\mathbf{T}_\infty} + \mathbf{D}_B\boldsymbol{\nabla}^2\mathbf{C}\ . \tag{2.39}$$

2.28 Thermal diffusivity

It is specific property of a material for relating the unsteady conductive heat flow. This value describes the responding speed of a material to change in temperature. It is the ratio between thermal conductivity to specific heat capacity and density. Mathematically,

$$\alpha^* = \frac{k}{\rho c_p}, \tag{2.40}$$

SI unit is $m^2/\sec$

2.29 Thermal conductivity

The ability of conducting heat of a substance is named as thermal conductivity. From the Fourier's law of heat conduction, "The amount of heat transfer rate Q through a material of unit thickness d times unit cross section area A and unit temperature difference ΔT". Mathematically, written as:

$$k = \frac{Qd}{A(\Delta T)}. \tag{2.41}$$

In SI system thermal conductivity has unit $\frac{W}{m.K}$.

Chapter 3

Impact of nonlinear radiation and entropy optimization coatings with hybrid nanoliquid flow past a curved stretched surface

This chapter is consist of review paper authored by Lu et.al published in 2018.

3.1 Mathematical formulation

In this chapter, two-dimensional steady, incompressible nanofluid flow on a curved stretching sheet of radius R^* about r and $x-$directions is assumed (see Fig 1). Here, $U = u_w$ is the stretching velocity along $x-$direction. A magnetic field of strength B_0 is activated in $r-$direction which is perpendicular to the stretching sheet (fluid flow). By taking small Reynolds number, the electric and induced magnetic fields are neglected.

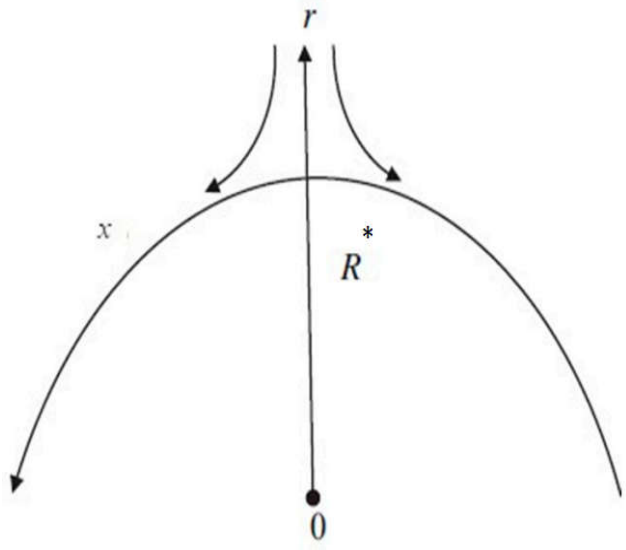

Figure 3.1. Geometry of flow.

The governing system of equations for present flow are:

$$R^*\frac{\partial U}{\partial x}+\frac{\partial}{\partial r}\{(r+R^*)v\}=0, \tag{3.1}$$

$$\frac{1}{\rho_{nf}}\frac{\partial p}{\partial r}=\frac{U^2}{R^*+r}, \tag{3.2}$$

$$v(\frac{\partial U}{\partial r})+\frac{UR^*}{r+R^*}(\frac{\partial U}{\partial x})+\frac{Uv}{R^*+r}=-\frac{1}{\rho_{nf}}(\frac{R^*}{r+R^*})\frac{\partial p}{\partial x}$$

$$+\frac{\mu_{nf}}{\rho_{nf}}\left\{\frac{\partial^2 U}{\partial r^2}+\frac{1}{r+R^*}(\frac{\partial U}{\partial r})-\frac{U}{(r+R^*)^2}\right\}-\frac{\sigma}{\rho_{nf}}B_0^2U, \tag{3.3}$$

$$v(\frac{\partial T}{\partial r})+\frac{UR^*}{r+R^*}(\frac{\partial T}{\partial x})=\alpha_{nf}\ \left\{(\frac{\partial^2 T}{\partial r^2}+\frac{1}{r+R^*}(\frac{\partial T}{\partial r})\right\}$$

$$+\frac{Q_0}{(\rho C_p)_{nf}}(T_\infty-T)+\frac{1}{(\rho C_p)_{nf}}(\frac{1}{r+R^*})\frac{\partial}{\partial r}(r+R^*)q_r, \tag{3.4}$$

$$\frac{UR^*}{r+R^*}(\frac{\partial C}{\partial x})+v(\frac{\partial C}{\partial r})=D_B(\frac{\partial^2 C}{\partial r^2}+\frac{1}{R^*+r}\frac{\partial C}{\partial r}), \tag{3.5}$$

with boundary conditions

$$U=u_w(x)=sx\ ,\ kf(\frac{\partial T}{\partial r})=-h^*\,(T-T_f)\quad ,\ v=0,$$

$$-D_B(\frac{\partial C}{\partial r})=j_w\qquad \text{at}\qquad r=0,$$

$$U\to 0\ \ ,\ \frac{\partial U}{\partial r}\to 0\ ,\ \ C\to C_\infty,\ T\to T_\infty\quad \text{as}\ \ r\to\infty. \tag{3.6}$$

Table-3.1 Thermo-physical properties of ethylene glycol and $NiZnFe_2O_4$(Nickle-Zinc Ferrite).

Thermophysical characteristics of	k (W/mK)	C_ρ (J/kg K)	ρ (kg/m^3)	P_r
ethylene glycol($C_2H_6O_2$)	0.2490	2382.0	1116.6	204.0
nickle-zinc ferrite($NiZnFe_2O_4$	6.3	710.0	4800.0	_

Thermophysical properties in mathematical form are:

$$\mu_{nf}=\frac{\mu_f}{(1-\Phi)^{\frac{25}{10}}},\ \alpha_{nf}=\frac{k_{nf}}{(\rho C_p)_{nf}}, \tag{3.7}$$

$$\rho_{nf}\ =(1-\Phi)\rho_f+\Phi\rho_s, \tag{3.8}$$

$$(\rho C_p)_{nf}=\ \Phi(\rho C_p)_s+(1-\Phi)\ (\rho C_p)_f, \tag{3.9}$$

$$\frac{k_{nf}}{k_f}\ =\ \frac{k_s+2k_f+2\Phi(k_s-k_f)}{k_s+2k_f-\Phi(k_s-k_f)}. \tag{3.10}$$

Term of nonlinear radiation heat flux via Rosseland's approximation, Eq.(3.4) is given as:

$$q_r=\frac{4\sigma^*}{3k^*}(\frac{\partial T^4}{\partial r})=\frac{16T^3\sigma^*}{3k^*}(\frac{\partial T}{\partial r}).$$

Now, we define the following dimensionless transformations:

$$\xi = \sqrt{\frac{s}{v_f}} r,\ p = \rho_f s^2 x^2 P(\xi), C = C_\infty - \frac{j_w}{D_B}\sqrt{\frac{v_f}{s}}\psi(\xi),$$

$$U = sxf'(\xi),\ v = -\frac{R^*}{R^*+r}\sqrt{sv_f} f(\xi),\ \ T = T_\infty\left[1+(\theta_w-1)\theta\right]. \tag{3.11}$$

Here, f' is the derivative w.r.t ξ and $\theta_w = \frac{T_f}{T_\infty}$. Eq. (3.1) is identically satisfied. However, Eqs.$(3.2)-(3.6)$ reduce:

$$P' = (1-\Phi+\Phi\frac{\rho_s}{\rho_f})\frac{f'^2}{\xi+K_1}, \tag{3.12}$$

$$\frac{1}{(1-\Phi+\Phi\frac{\rho_s}{\rho_f})}\frac{2K_1}{\xi+K_1}P = \frac{1}{(1-\Phi)^{\frac{25}{10}}(1-\Phi+\Phi\frac{\rho_s}{\rho_f})}$$
$$(f''' - \frac{f'}{(\xi+K_1)^2} + \frac{f''}{\xi+K_1}) - \frac{K_1}{\xi+K_1}f'^2$$
$$+\frac{K_1}{\xi+K_1}ff'' + \frac{K_1}{(\xi+K_1)^2}f'f - \frac{Ha}{1-\Phi+\Phi\frac{\rho_s}{\rho_f}}f', \tag{3.13}$$

$$\frac{1}{\Pr}\left(\frac{k_{nf}}{k_f} + R_d(1+(\theta_w-1)\theta)^3\right)\left(\theta'' + \frac{1}{\xi+K_1}\theta'\right) + \left(1-\Phi+\Phi\frac{(\rho C_p)_s}{(\rho C_p)_f}\right)$$

$$(\frac{K_1}{\xi+K_1}f\theta') - \lambda_1\theta + \frac{3}{\Pr}R_d(1+(\theta_w-1)\theta)^2\theta'^2(\theta_w-1) = 0, \tag{3.14}$$

$$\psi'' + \frac{1}{\xi+K_1}\psi' + S_c(\frac{K_1}{\xi+K_1})f\psi' = 0, \tag{3.15}$$

and

$$f(0) = 0,\ f'(0) = 1,\ \theta'(0) = -(1-\theta(0))Bi,\ \psi'(0) = -1,$$

$$f'(\infty)\to 0,\ f''(\infty)\to 0,\ \theta(\infty)\to 0,\ \psi(\infty)\to 0, \tag{3.16}$$

where

$$K_1 = R^*\sqrt{\frac{s}{\nu_f}}, \lambda_1 = \frac{Q_0}{s(\rho C_p)_f},\ Bi = \frac{h^*\sqrt{\frac{v_f}{s}}}{k_f},$$

$$\Pr = \frac{\nu_f}{\alpha_f}\ ,\ Sc = \frac{\nu_f}{D_B},\ R_d = \frac{16\sigma^* T_\infty^3}{3kk^*},\ Ha = \frac{\sigma B_0^2}{s\rho_f}. \tag{3.17}$$

Eliminating pressure between Eqs. (3.12) and (3.13), we get

$$f^{iv} + \frac{2f'''}{\xi + K_1} - \frac{f''}{(\xi + K_1)^2} + \frac{f'}{(\xi + K_1)^3} + (1-\Phi)^{2.5}(1 - \Phi + \Phi\frac{\rho_s}{\rho_f})$$
$$\{\frac{K_1}{(\xi + K_1)^2}(f'^2 - ff'') - \frac{K_1}{\xi + K_1}(f'f'' - ff''')$$
$$-\frac{K_1}{(\xi + K_1)^3}ff'\} - (1-\Phi)^{2.5}Ha(\frac{f'}{\xi + K_1} + f'') = 0. \tag{3.18}$$

with

$$f(\xi) = 0, f'(\xi) = 1,\ \text{as}\ \xi = 0\ \ \text{and}\ f'(\xi) \to 0, f''(\xi) \to 0,\ \text{as}\ \xi \to \infty. \tag{3.19}$$

Along x-direction the Nusselt number (Nu_x), Surface Drag coefficient (C_f) and Sherwood number (Sh_x) are:

$$C_f = \frac{\tau_{\mathbf{rx}}}{\frac{1}{2}\rho u_w^2},\quad Nu_x = \frac{xq_w}{k_f(T_f - T_\infty)}, Sh_x = -\frac{x}{(C - C_0)}\frac{\partial C}{\partial r}. \tag{3.20}$$

where

$$\tau_{rx} = \mu_{nf}(\frac{\partial U}{\partial r} - \frac{U}{R^* + r})\ |_{r=0}\ \ ,q_w = (q_r)_w - \frac{\partial T}{\partial r}\ |_{r=0}. \tag{3.21}$$

Finally, Equation (3.20) after using Eqs.(3.11) and (3.19)

$$\frac{1}{2}C_f\,\mathrm{Re}_x^{1/2} = \left(f'''(0) - \frac{f'(0)}{K_1}\right),\quad Sh_x(\mathrm{Re}_x)^{-\frac{1}{2}} = \frac{1}{\psi(0)},$$

$$Nu_x\,\mathrm{Re}_x^{-1/2} = -[\frac{k_{nf}}{k_f} + R_d(1 + (\theta_w - 1)\theta(0))^3]\theta'(0), \tag{3.22}$$

here, $\mathrm{Re}_x = \frac{sx^2}{\nu_f}$.

3.2 Entropy Generation

The dimensional form of entropy generation equation is:

$$E'''_{gen} = \frac{k_{nf}}{T_f^2}[(\frac{\partial T}{\partial r})^2 + \frac{16\sigma^* T^3}{3k_{nf}k^*}(\frac{\partial T}{\partial y})^2] + \frac{\mu_{nf}}{T_f}(\frac{\partial U}{\partial r})^2,$$
$$+\frac{\sigma B_0^2}{T_f}U^2 + \frac{Rd}{C_\infty}(\frac{\partial C}{\partial r})^2 + \frac{Rd}{T_f}(\frac{\partial C}{\partial r})(\frac{\partial T}{\partial r}). \tag{3.23}$$

After applying dimensionless transformations, Equation (3.23) reduces in to following form:

$$N_G = \frac{E'''_{gen}}{E'''_0} = \mathrm{Re}_x[\frac{\mathbf{k}_{nf}}{\mathbf{k}_f} + R_d(1+\Pi\theta)^3]\theta'^2,$$
$$+\frac{Br\,\mathrm{Re}_x}{\Pi^2}[(f'')^2 + Haf'^2] + \frac{\mathrm{Re}_x \sum}{\Pi}(\psi'^2 + \frac{\theta'\psi'}{\Pi}), \tag{3.24}$$

here,

$$Br = \frac{\mu_{nf}u_w^2}{k_{nf}T_f}, \quad \mathrm{Re}_x = \frac{x^2 s}{v_f}, \quad \sum = \frac{C_\infty RD}{k_{nf}}, \quad \Pi = \theta_w - 1. \tag{3.25}$$

3.3 Results and discussion

The bvp4c MATLAB scheme is used to integrate the numerical solution for system of Eqs. $(3.14)-(3.15)$ and (3.18) with initial and boundary conditions. Eqs. $(3.16)-(3.19)$ for several values of K_1, M, R_d, λ_1, and S_c graphically. For this method by using new variables we can obtain first order differential equations from higher order. The tool bvp4c for solution with the tolerance of 10^{-7}usess an initial guess. The selected guess must satisfy the Equations (3.16) and (3.18) *i.e.* boundary conditions and the solution. A magnificent bond with Sanni et al. [50] is observed in the absence of concentration and temperature profile when $Ha = 1$ and $\Phi = 0.0$.

Table 3.2: Result comparison of skin drag force $\frac{1}{2}C_f(\mathrm{Re})^{\frac{1}{2}}$when $Ha = 1$, $\Phi = 0.0$

K_1	Sanni et al. [50]	Present Result
5	1.1576	1.15760
10	1.0734	1.07341
20	1.0355	1.03540
50	1.0140	1.01400
100	1.0070	1.00690
1000	1.0008	1.00079

Figures 3.2 and 3.3 are shown the influnce of solid volume fraction on velocity and temperature profiles. Fields of velocity and temperature increases with increasing values of solid volume fraction. Moreover, the thermal boundary layers thickness and the momentum are improved with larger values of Φ . The values of parameters are $\mathrm{Pr} = 10$, $K_1 = 10$, $\theta_w = R_d = S_c = \lambda_1 = 0.5$ and $Ha = \Phi = Bi = 0.1$. The impact of the curvature parameter K_1 on the velocity, concentration and temperature profiles is shown in Figures 3.4-3.6. As K_1 increases, the velocity and temperature of the liquid increase with decreasing concentration field. Physically, radius of the surface increases as (K_1) curvature parameter increases, which causes greater resistance in the flow rate. Hence, temperature increases. Figure 3.7 is ploted to show the change in the velocity gradient for higher estimates of the magnetic field Ha. Here an increase in Ha leads to a decrease in the velocity of the fluid. This is caused by the resistance of the magnetic field (Lorentz force), which reduces flow rate of the fluid. Figures 3.8 and 3.9 demonstrate the features of Biot number (Bi) and heat generation parameter $\lambda_1$on temperature field respectively. Figure 3.8 shows that the convective heat transfer coefficient increases and the temperature raises with higher values of Bi. Figure 3.9 shows the behavior of λ_1, to increase the heat generation absorption values, the temperature profile and the thermal boundary layer thickness are increased. The values of other parameters are fixed as $Ha = 0.3$, $\Phi = \theta_w = 0.5$, $R_d = Bi = 0.1$, $S_c = 5$ and $K_1 = \mathrm{Pr} = 10$. Figures 3.10 and 3.11 show

the effect of nonlinear radiation parameters R_d and Pr (Prandtl number) on temperature distribution. The temperature field decreases as the Prantle number increases. Due to the reciprocal link between thermal diffusivity and Prandtl number, a rapid addition in the Prandtl number Pr reduce the temperature and thermal boundary layer thickness. The temperature profile increases with larger estimates of nonlinear radiation parameter (R_d). Physically, the radiant heat flux increases with higher values of R_d and eventually increases the fluid temperature. The increase in the Schmidt number S_c for the concentration distribution is drawn in Figure 3.12. A reduction in the concentration profile with increasing S_c is noticed. Since the Schmidt number and the Brownion diffusion coefficient are inversely proportional to each other, so an enhancement in the S_c reduces the Brownian diffusion coefficient and decreases the concentration and thickness of the interconnected boundary layer. Figure 3.13 shows the relationship between the entropy generation and the magnetic parameter Ha. the same features are noticed as in case of Brinkman number (Br). Increasing Ha means that the Lorentz force increases and eventually dissipaton energy increases, which is the main cause of irreversibility. The effect of Brinkman number (Br) on entropy generation is examined in Figure 3.14. From the Figure it can be seen that optimization of entropy increases with increasing values of Br. This is due to the fact that the augmented value of (Br), more heat is emitted/generated between the layers of the liquid. Table 3.3 specifies the effect of magnetic parameter Ha and curvature parameter K_1 on surface drag force $-\frac{1}{2}C_f(R_{e_x})^{\frac{1}{2}}$. It can be seen that increasing the K_1 values reduce the Skin friction coefficient. An opposite trend is demonstrated in case of Ha. The up shot of magnetic parameter Ha and solid volume fraction Φ on shear wall stress are also illustrated in it. The Skin drag force coefficient rises with increase in solid volume fraction Φ for fixed values of other parameters as Pr = 10, $S_c = 0$. The Skin drag force coefficient remains constant for increasing values of magnetic parameter Ha. Table 3.4 also shows the behavior of the Sherwood numbers $Sh_x(\mathrm{Re}_x)^{-\frac{1}{2}}$for different values of Sc (Schmidt number), K_1 (The curvature parameter) and Ha (magnetic parameter) in case of rapid increasing values of (S_c), the Sherwood

number $Sh_x(\mathrm{Re}_x)^{-\frac{1}{2}}$ increases, However it decreases for increasing values of $K_1$and Ha. Table 3.3 demonstrates the influence of the Biot number Bi and solid volume fraction Φ on Nusselt number $Nu_x(\mathrm{Re}_x)^{\frac{-1}{2}}$. It is noticed that for greater values of Φ and Bi, the rate of surface heat transfer increases for fixed values of other parameters. The result of curvature parameter K_1 and nonlinear radiation parameter R_d on Nusselt number is analyzed in Table 3.3. As discussed in the table, decrease in Nusselt number and the opposite tendency is noticed for nonlinear radiation parameter R_d for increasing values of curvature parameter K_1 for fixed values of Ha, S_c, Φ, θ_w, λ_1 and $\mathrm{Pr} = 10$.

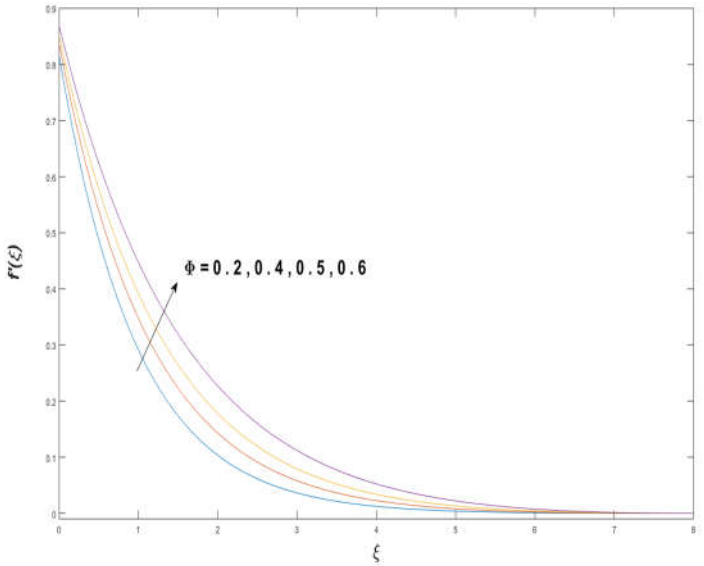

Figure 3.2: Effect of Φ on $f^{'}(\xi)$.

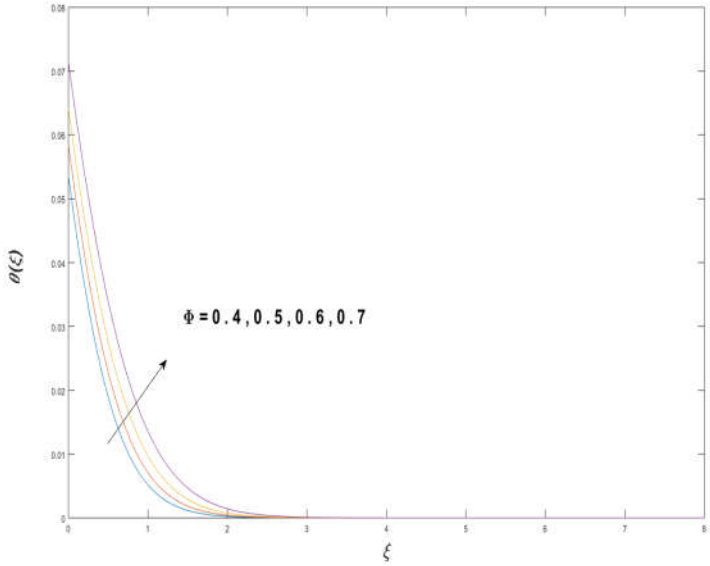

Figure 3.3: Effect of Φ on $\theta(\xi)$.

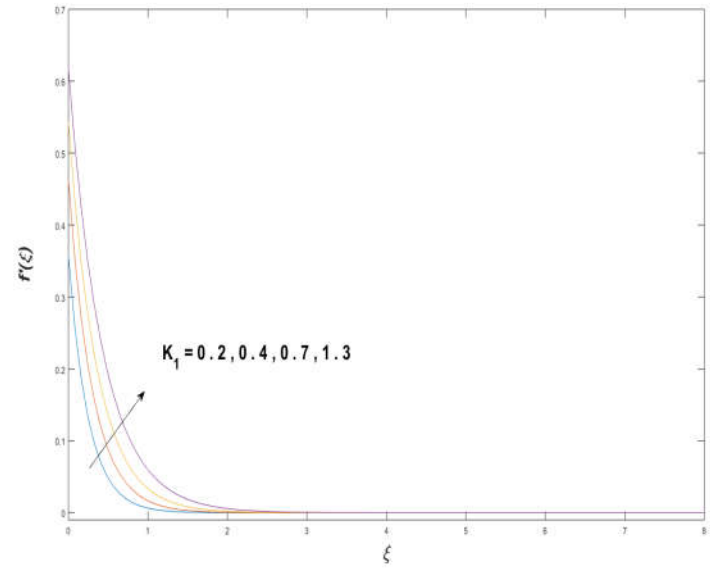

Figure 3.4: Effect of K_1 on $f^{'}(\xi)$.

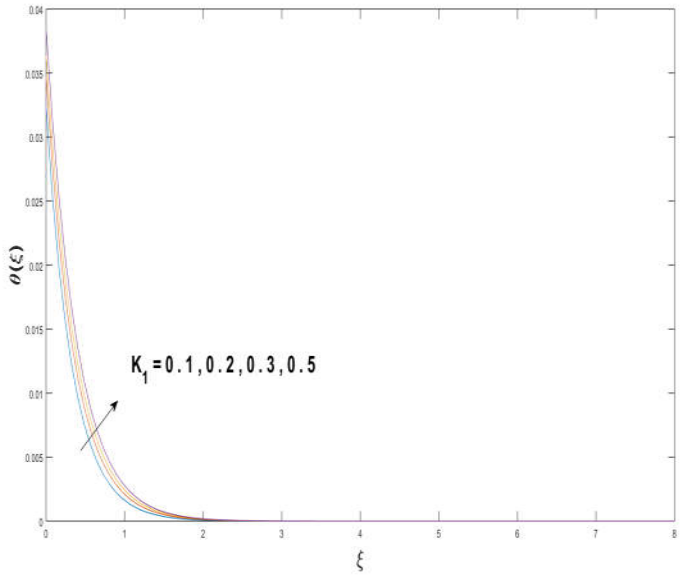

Figure 3.5. Effect of K_1 on $\theta(\xi)$

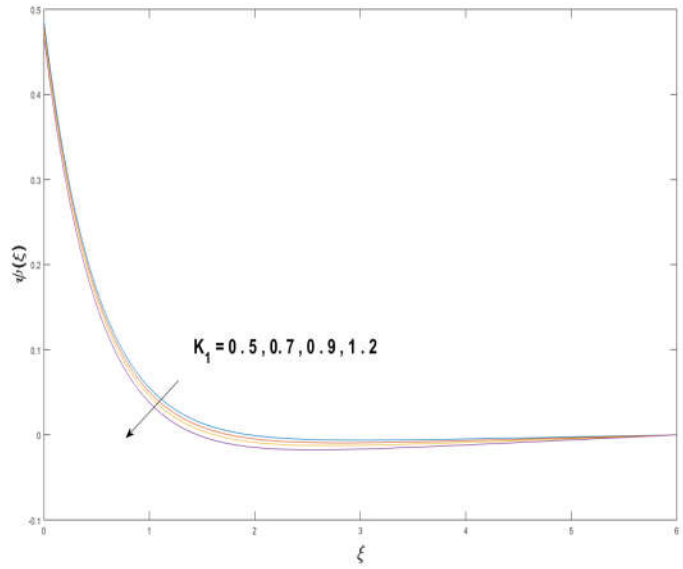

Figure 3.6: Effect of K_1 on $\psi(\xi)$.

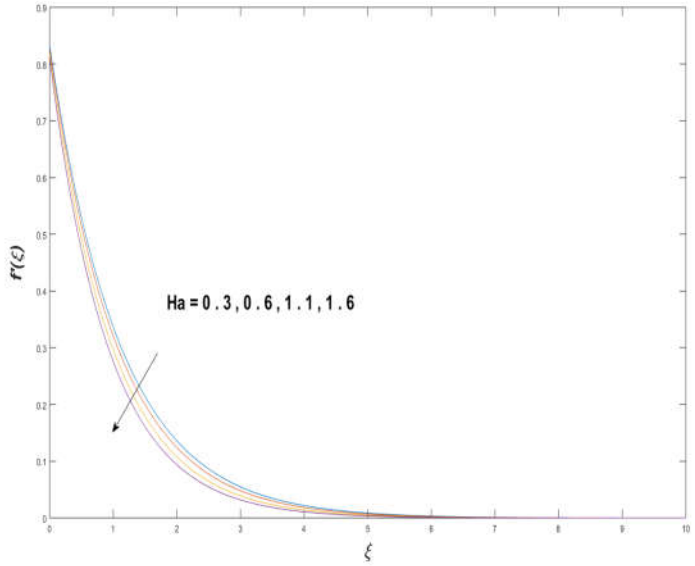

Figure 3.7. Effect of Ha on $f'(\xi)$

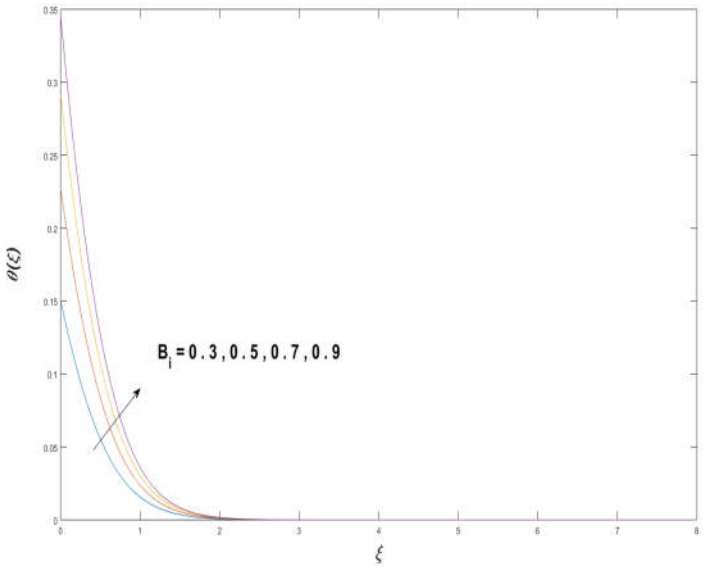

Figure 3.8. Effect of Bi on $\theta(\xi)$

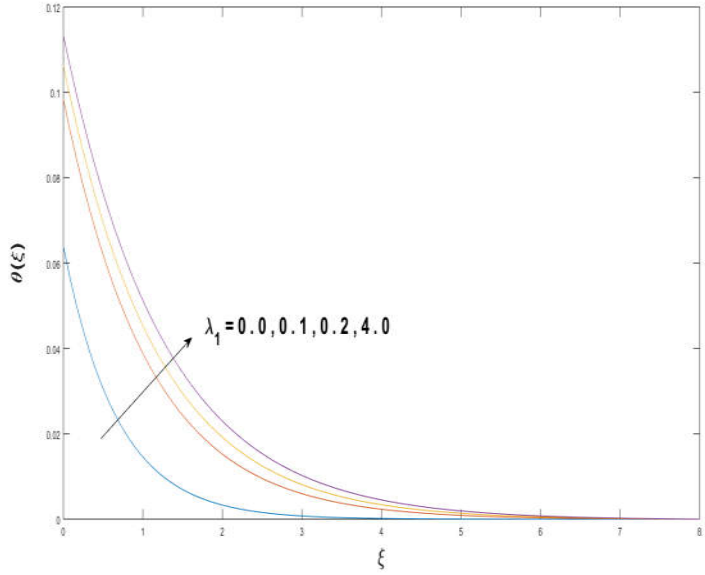

Figure 3.9. Effect of λ_1 on $\theta(\xi)$

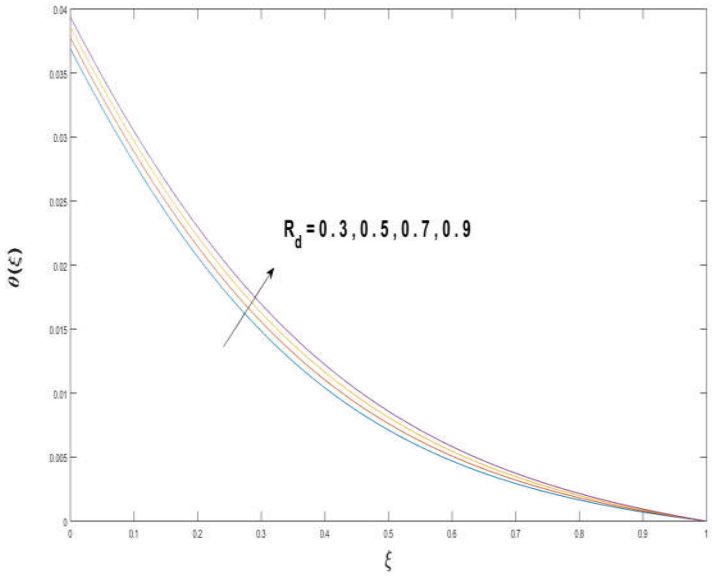

Figure 3.10. Effect of R_d on $\theta(\xi)$

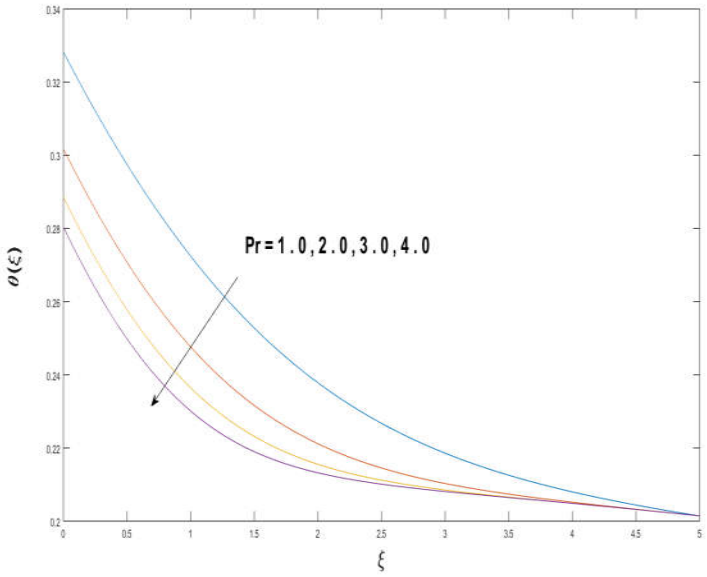

Figure 3.11. Effect of Pr on $\theta(\xi)$

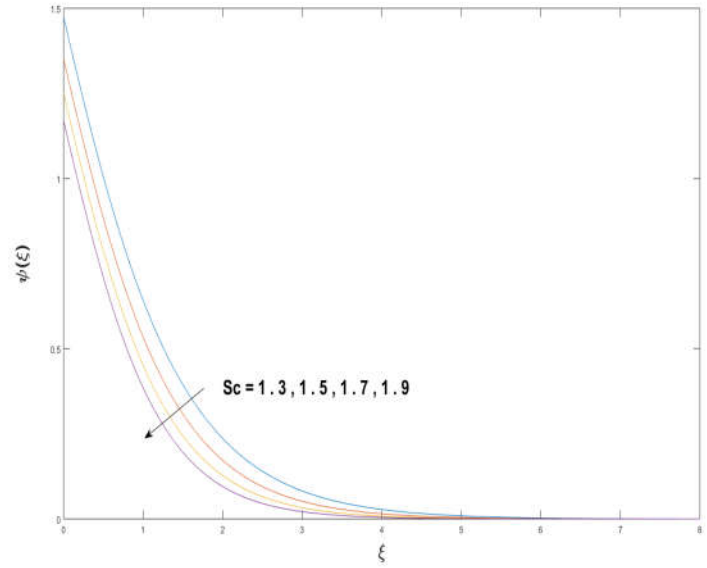

Figure 3.12. Effect of Sc on $\psi(\xi)$.

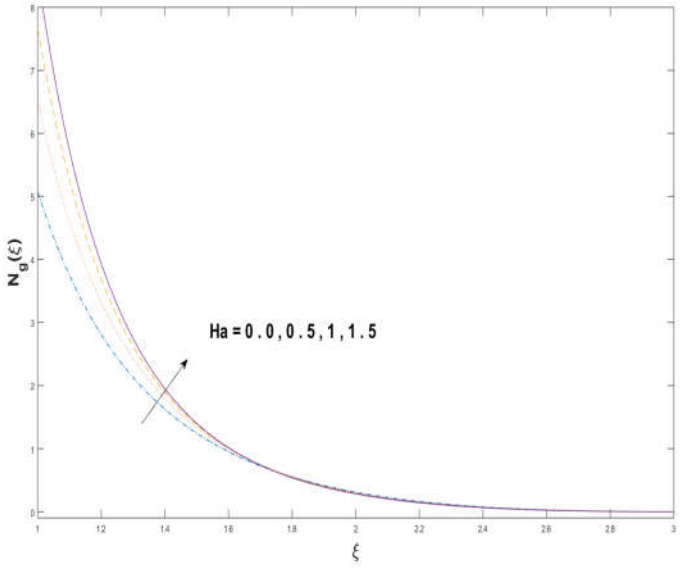

Figure 3.13. Effect of Ha on entropy generation.

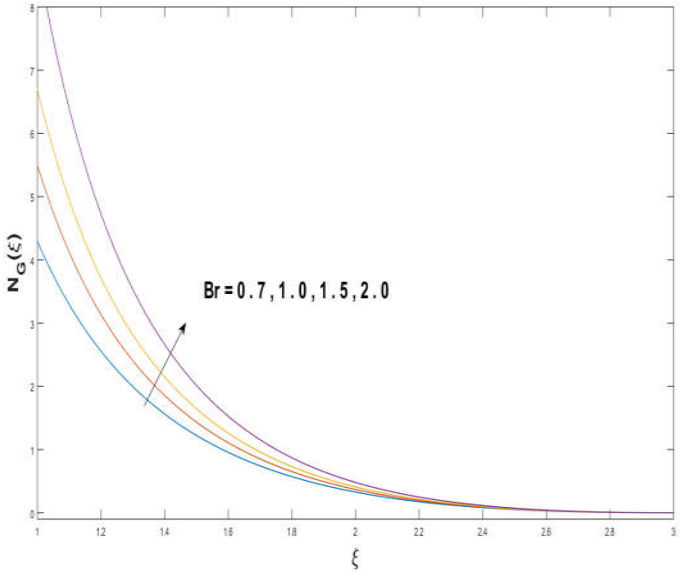

Figure 3.14. Effect of Br on entropy generation.

Table 3.3: Numerical values of Skin drag force $-\frac{1}{2}C_f(\mathrm{Re}_x)^{\frac{1}{2}}$and Nusselt number.

$K1$	Ha	Φ	Bi	R_d	λ_1	θ_w	$-\frac{1}{2}C_f(\mathrm{Re}_x)^{\frac{1}{2}}$	$Nu(\mathrm{Re}_x)^{\frac{-1}{2}}$
0.8	0.4	0.5		0.5	0.5	0.5	5.7470	0.3237
1.0							5.6241	0.3233
1.3							5.3590	0.3229
0.8	0.1						5.74700	0.3237
	0.3						5.7891	0.3237
	0.5						5.8312	0.3237
	0.1	0.02					1.2382	0.1017
		0.2					2.0152	0.1584
		0.5					5.7470	0.3237
		0.5	0.7				-	1.7582
			1.0				-	2.2651
			1.5				-	2.9260
			2.0	0.1			-	3.4143
				0.3			-	3.4228
				0.5			-	3.4314
				0.7	0.7		-	3.5757
					0.9		-	3.6891
					1.0		-	3.7395
					0.7	0.5	-	3.5757
						0.7	-	3.5587
						0.9	-	3.5333
						1.0	-	3.1573

Table 3.4 Numerical values of Sherwood numbers $Sh_x(\mathrm{Re}_x)^{-\frac{1}{2}}$for various values of Sc,K_1, M with fixed values of $\mathrm{Pr} = 10, R_d = 0.1, \Phi = 0.1, Bi = 0.1, \theta_w = 0.5, \lambda_1 = 0.5$

Sc	K_1	Ha	$Sh_x(\mathrm{Re}_x)^{-\frac{1}{2}}$
0.5	10	0.1	0.38325
1.0	–	–	0.59354
2.0	–	–	0.92268
5	5	0.1	1.60150
–	10	–	1.58090
–	50	–	1.56230
5	10	0.3	1.56270
–	–	0.5	1.54600
–	–	0.7	1.53040

Chapter 4

A numerical simulation of hybrid nanofluid flow with homogenous-heterogenous reactions over a curved surface

4.1 Mathematical modelling

In this chapter, we consider an incompressible 2D nanofluid flow over a curved steady stretching sheet coiled in a semi-circle of radius R^*. The stretching sheet is in the $x-$direction with velocity $U = u_w$. In $r-$direction the induced magnetic field of strength B_0 is enforced $i.e$, perpendicular to the fluid flow. Temperature T of sheet is kept constant while T_∞ is ambient temperature of fluid. The process of heat transfer is exaimned through heat absorption/generation effects. Homogenous-heterogenous reactions of two chemical species A and B are considered. For cubic autocatalysis, the homogenous reaction can be defined as:

$$A + 2B \rightarrow 3B, \qquad \text{rate} = k_c c_1 c_2^2. \tag{4.1}$$

while the heterogenous reaction on reactant surface is

$$A \to B, \qquad \text{rate} = k_s c_1. \tag{4.2}$$

Here, c_1, c_2 are the concentrations of chemical species A and B respectively and k_c, k_s are the rate constants.

The continuity, momentum, energy and homogenous heterogenous reactions equations are:

$$R^*(\frac{\partial U}{\partial x}) + \frac{\partial}{\partial r}\{(r+R^*)v\} = 0, \tag{4.3}$$

$$\frac{U^2}{r+R^*} = \frac{1}{\rho_{nf}}(\frac{\partial p}{\partial r}), \tag{4.4}$$

$$v(\frac{\partial U}{\partial r}) + \frac{UR^*}{r+R^*}(\frac{\partial U}{\partial x}) + \frac{Uv}{r+R^*} = -\frac{1}{\rho_{nf}}(\frac{R^*}{r+R^*})(\frac{\partial p}{\partial x})$$
$$+\frac{\mu_{nf}}{\rho_{nf}}\{\frac{\partial^2 U}{\partial r^2} + \frac{1}{r+R^*}(\frac{\partial U}{\partial r}) - \frac{U}{(r+R^*)^2}\} - \frac{\sigma}{\rho_{nf}}B_0^2 U, \tag{4.5}$$

$$v(\frac{\partial T}{\partial r}) + (\frac{UR^*}{r+R^*})(\frac{\partial T}{\partial x}) = \alpha_{nf}\{\frac{\partial^2 T}{\partial r^2} + \frac{1}{r+R^*}(\frac{\partial T}{\partial r})\}$$
$$+\frac{Q_0}{(\rho C_p)_{nf}}(T_\infty - T) + \frac{1}{(\rho C_p)_{nf}}(\frac{1}{R^*+r})\frac{\partial}{\partial r}(R^*+r)q_r, \tag{4.6}$$

$$v(\frac{\partial c_1}{\partial r}) + \frac{R^*U}{R^*+r}(\frac{\partial c_1}{\partial x}) = Dc_1\{\frac{\partial^2 c_1}{\partial r^2} + \frac{1}{R^*+r}(\frac{\partial c_1}{\partial r})\} - k_c c_1 c_2^2, \tag{4.7}$$

$$v(\frac{\partial c_2}{\partial r}) + \frac{UR^*}{r+R^*}(\frac{\partial c_2}{\partial x}) = Dc_2\{\frac{\partial^2 c_2}{\partial r^2} + \frac{1}{r+R^*}(\frac{\partial c_2}{\partial r})\} + k_c c_1 c_2^2, \tag{4.8}$$

with the subjected conditions

$$U|_{r=0} = xs + L[\frac{\partial U}{\partial r} - \frac{U}{r+R^*}],\ v|_{r=0} = 0, k_f(\frac{\partial T}{\partial r})|_{r=0} = h^*\left(T_f - T\right),$$

$$Dc_1\frac{\partial c_1}{\partial r}|_{r=0} = k_s c_1, \qquad Dc_2\frac{\partial c_2}{\partial r}|_{r=0} = -k_s c_1$$

$$U \to 0 \quad , \ \frac{\partial U}{\partial r} \to 0 \quad , \ T \to T_\infty \ , c_1 \to c_0, \quad c_2 \to 0 \quad \text{as} \quad r \to \infty. \tag{4.9}$$

Invoking the following transformations

$$\xi = \sqrt{\frac{s}{\nu_f}}r, \quad p = \rho_f s^2 x^2 P(\xi),$$

$$\begin{aligned} T &= T_\infty(1+(\theta_w-1)\theta), \ U = sxf'(\xi), \ c_1 = c_0\psi(\xi) \\ c_2 &= c_0 g(\xi), \quad v = -\frac{R^*}{r+R^*}\sqrt{sv_f}f(\xi), \ \ \theta_w = \frac{T_f}{T_\infty}. \end{aligned} \tag{4.10}$$

After using boundary layer approximation and invoking here, Eq. (4.3) is automatically satisfied and remaining, Eqs. $(4.4)-(4.9)$ take the form:

$$P' = (1-\Phi+\Phi\frac{\rho_s}{\rho_f})\frac{f'^2}{\xi+K_1}, \tag{4.11}$$

$$\frac{1}{(1-\Phi+\Phi\frac{\rho_s}{\rho_f})}\frac{2K_1}{\xi+K_1}P = \frac{1}{(1-\Phi)^{\frac{25}{10}}(1-\Phi+\Phi\frac{\rho_s}{\rho_f})}$$

$$\left[f''' - \frac{f'}{(\xi+K_1)^2} + \frac{f''}{\xi+K_1}\right] - \frac{K_1}{\xi+K_1}f'^2$$

$$+\frac{K_1}{\xi+K_1}ff'' + \frac{K_1}{(\xi+K_1)^2}f'f - \frac{Ha}{1-\Phi+\Phi\frac{\rho_s}{\rho_f}}f', \tag{4.12}$$

$$\frac{1}{\mathrm{Pr}}(\frac{k_{nf}}{k_f} + R_d((\theta_w-1)\theta+1)^3(\theta'' + \frac{1}{\xi+K_1}\theta')$$

$$+(1-\Phi+\Phi\frac{(\rho C_p)_s}{(\rho C_p)_f})(\frac{K_1}{\xi+K_1}f\theta')$$

$$-\lambda_1\theta + \frac{3}{\mathrm{Pr}}R_d(1+(\theta_w-1)\theta)^2\theta'^2(\theta_w-1) = 0, \tag{4.13}$$

$$\frac{1}{S_c}(\psi'' + \frac{1}{\xi + K_1}\psi') + \frac{K_1}{\xi + K_1} f\psi' - k_1\psi g^2 = 0, \tag{4.14}$$

$$\frac{\delta}{S_c}(g'' + \frac{1}{\xi + K_1}g') + \frac{K_1}{\xi + K_1} fg' + k_1\varphi g^2 = 0, \tag{4.15}$$

with

$$f(\xi) = 0, , f''(\xi) = 0, \theta(\xi) = 0, \quad f'(\xi) = 1 + \mathbf{K}^*[f''(\xi) - f'(\xi)/K_1],$$

$$\theta'(\xi) = Bi\,(1 - \theta(\xi)), \psi'(\xi) = k_2\psi(\xi),\ \delta g'(\xi) = -k_2\psi(\xi),\ \text{at} \quad \xi = 0 \tag{4.16}$$

$$f'(\infty) \to 0,\ f''(\infty) \to 0,\ \theta(\infty) \to 0. \tag{4.17}$$

These parameters are mathematically defined as:

$$\begin{aligned} K_1 &= R^*\sqrt{\frac{s}{v_f}}, \qquad Bi = h^*\frac{\sqrt{\frac{v_f}{s}}}{k_f}, \quad S_c = \frac{v_f}{Dc_1}, \qquad R_d = \frac{16\sigma^* T_\infty^3}{3k^* k}, \qquad \mathrm{Pr} = \frac{v_f}{\alpha}, \\ \lambda_1 &= \frac{Q_0^*}{s(\rho C_p)_f},\ Ha = \sigma\frac{B_0^2}{s\rho_f}, k_1 = c_0^2\frac{k_c}{s}, k_2 = \frac{k_s\sqrt{\frac{v_f}{s}}}{Dc_1}, \delta = \frac{Dc_2}{Dc_1}, \mathbf{K}^* = L\sqrt{\frac{s}{v_f}}. \end{aligned} \tag{4.18}$$

Eliminating pressure from Eqs.(4.11) − (4.12), we get

$$f^{iv} + \frac{2f'''}{\xi + K_1} - \frac{f''}{(\xi + K_1)^2} + \frac{f'}{(\xi + K_1)^3} + (1 - \Phi)^{2.5}\left[1 - \Phi + \Phi\frac{\rho_s}{\rho_f}\right]$$

$$\left\{\frac{K_1}{(\xi + K_1)^2}(f'^2 - ff'') - \frac{K_1}{\xi + K_1}(f'f'' - ff''') - \frac{K_1}{(\xi + K_1)^3}f'f\right\}$$

$$-(1 - \Phi)^{2.5} Ha\left[\frac{f'}{\xi + K_1} + f''\right] = 0. \tag{4.19}$$

Thermophysical properties in mathematical form are given as:

$$\mu_{nf} = \frac{\mu_f}{(1 - \Phi)^{\frac{25}{10}}}, \tag{4.20}$$

$$\alpha_{nf} = \frac{k_{nf}}{(\rho C_p)_{nf}}, \tag{4.21}$$

$$\rho_{nf} = \Phi\rho_s + (1-\Phi)\rho_f, \tag{4.22}$$

$$(\rho C_p)_{nf} = \ \Phi(\rho C_p)_s + (1-\Phi)\ (\rho C_p)_f, \tag{4.23}$$

$$\frac{k_{nf}}{k_f} = \ \frac{k_s + 2k_f + 2\Phi(k_s - k_f)}{k_s + 2k_f - \Phi(k_s - k_f)}. \tag{4.24}$$

When the diffusion coefficients $Dc_1 = Dc_2$, then $\delta = 1$, we have

$$\psi(\xi) + g(\xi) = 1. \tag{4.25}$$

Then Equations (4.14) and (4.15) become

$$\frac{1}{S_c}(\psi'' + \frac{1}{\xi + K_1}\psi') + \frac{K_1}{\xi + K_1} f\psi' - k_1\psi(1-\psi)^2 = 0, \tag{4.26}$$

with boundary conditions

$$\psi'(0) = k_2\psi(0), \quad \psi(\infty) \to 1. \tag{4.27}$$

Along $x-$direction, Nusselt number(Nu_x), surface drag force (C_f) are in

$$Nu_x = \frac{xq_r}{k_f\,(T_f - T_\infty)}, C_f = \frac{2\tau_{rx}}{u_w^2\rho}, \tag{4.28}$$

$$\tau_{rx} = \mu_{nf}(\frac{\partial U}{\partial r} - \frac{U}{R^* + r})|_{r=0}, (q_r)_w = q_w + (\frac{\partial T}{\partial r})|_{r=0}. \tag{4.29}$$

Nusselt number and surface drag force in dimensionless form are appended as follows:

$$Nu_x(\mathrm{Re}_x)^{\frac{-1}{2}} = -\left[\frac{k_{nf}}{k_f} + Rd1 + (\theta_w - 1)\,\theta\,(0)\right]^3 \theta'\,(0)\,,$$

$$\frac{1}{2}C_f(\mathrm{Re}_x)^{\frac{1}{2}} = f''(0) - \frac{f'(0)}{K_1}. \tag{4.30}$$

The local Reynolds number is expressed as $\mathrm{Re}_x = \frac{sx^2}{\nu_f}$.

4.2 Results and discussion

We compute the velocity profile, temperature distribution and heat transfer characterized by solving Eqs. $(4.12) - (4.13), (4.19), (4.26)$ subjected to boundary conditions $(4.16) - (4.17)$ and (4.27) by using tool $MATLAB$ build-in function $bvp4c$. This particular section is dedicated to envision the impact of different parameters, on the velocity $f'\,(\xi)$, temperature $\theta\,(\xi)$ and concentration profiles $\psi\,(\xi)$. Figures 4.2 and 4.3 are illustrated to see the effects of volume fraction Φ on the temperature and velocity fields. The magnitude of fluid velocity and temperature field increase with increasing values of Φ. The momentum boundary layer thickness is getting higher for larger values of Φ. The values of other parameters are fixed as $\mathrm{Pr} = K_1 = 10$, $Sc = 0.5$, $R_d = 1.5$, $\lambda_1 = 10.5$ and $Ha = \Phi = 0.1$. Figure 4.3 is sketched to see the effect of curvature parameter K_1 on the velocity profile $f'(\xi)$. The velocity of the fluid increases with increasing value of K_1. The radius of surface increase for higher values of curvature parameter K_1, which enhances the fluid velocity. Figure 4.4 demonstrates the behaviour of the temperature distribution for various values of K_1. It is observed from this figure that higher values of K_1 cause an increase in temperature as well as in thermal boundary layer. Figure 4.5 elucidates the influence of magnetic parameter Ha on velocity distribution $f'(\xi)$. A decline in the magnitude of velocity is subjected to the enhance values of Hartman number Ha. This is because, the external magnetic field acts as a resistive force (Lorentz force) to the fluid velocity. Figures 4.6 and 4.7 illustrate the characteristic of Bi (Biot number)

and heat source (generation/absorption) parameter λ_1 on temperature distribution $\theta(\xi)$, respectively. Figure 4.6 depicts that the convective heat transfer coefficient augments for higher values of Bi and the temperature eventually boosted. Figure 4.7 demonstrates the temperature field affected by λ_1. So, by increasing the values of λ_1 temperature and thermal boundary layer thickness increase. Figure 4.8 gives the change of radiation parameter R_d on dimensionless temperature $\theta(\xi)$. Enhancement in temperature profile is noticed for increasing values of nonlinear radiation parameter R_d. Physically, the conduction effects (radiative heat flux) enhance for increasing values of R_d which causes the increase in temperature of the fluid. Figure 4.9 displays the effect of Prandtl number Pr on temperature distribution. It is evident from this figure that the temperature profile decreases with the increasing values of Pr, because the thermal diffusitivity and Prandtl number are connected reciprocally. As the increase in Pr causes reduction in temperature as well as in boundary layer thickness. The impact of curvature parameter K_1 on concentration distribution is depicted in Figure 4.10. It shows that concentration field reduces for higher values of curvature parameter K_1. Figure 4.11 portrays a decline in concentration $\psi(\xi)$ with increasing values of Schmidt number. The relation between mass diffusivity and viscosity is called Schmidt number S_c. Then mass diffusivity decreases with increasing Schmidt number. Consequently, reduction in concentration of fluid. Figure 4.12 specifies that concentration field $\psi(\xi)$ decreases with high strength of homogenous reaction parameter k_1. Actually, the reactants are consumed during homogenous reaction. Concentration profile for larger strength of heterogenous reaction parameter k_2 is explained in Figure 4.13. When k_2 increases, the concentration profile decreases because of reduction in diffusion. Concentration profile for larger strength of heterogenous reaction parameter k_2 is explained in Figure 4.13. When k_2 increases, the concentration profile reduces because of reduction in diffusion. Other parameters are fixed as $K = 0.5$, $Sc = 1.5$, $Ha = 0.3$, $k_1 = 0.9$, $Rd = Bi = 0.1$. Table 4.1 shows the influence of various parameters on Skin drag force coefficient and Nusselt number. Drag force coefficient increases for larger values of Ha (Hartmann number), Φ (solid vol-

ume fracition of nanofluid) and K_1(curvature parameter). Gradually reduction of Nusselt number is noticed for higher values of K_1. Both Nusselt number and Skin friction coefficient increases for larger values of solid volume fricition Φ of nanofluid. For higher values of Radiation parameter R_d, Biot number Bi, λ_1 and θ_w heat transmission rate enhance and no influence on skin fricition coefficient.

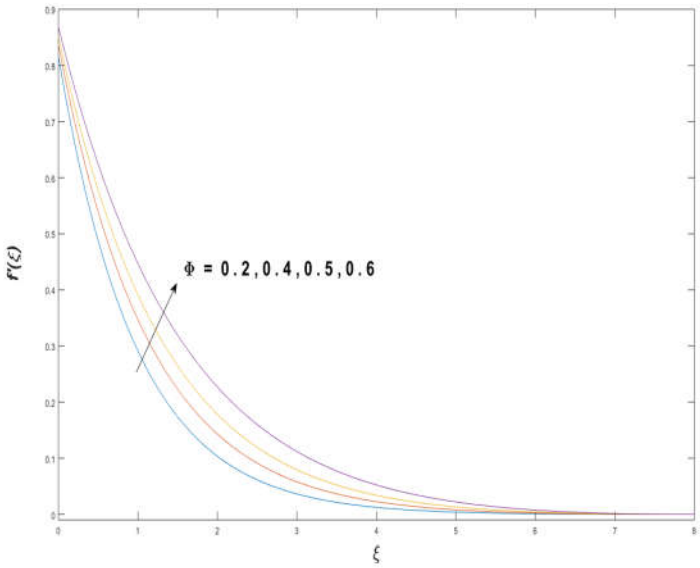

Figure 4.1: Effect of Φ on $f'(\xi)$.

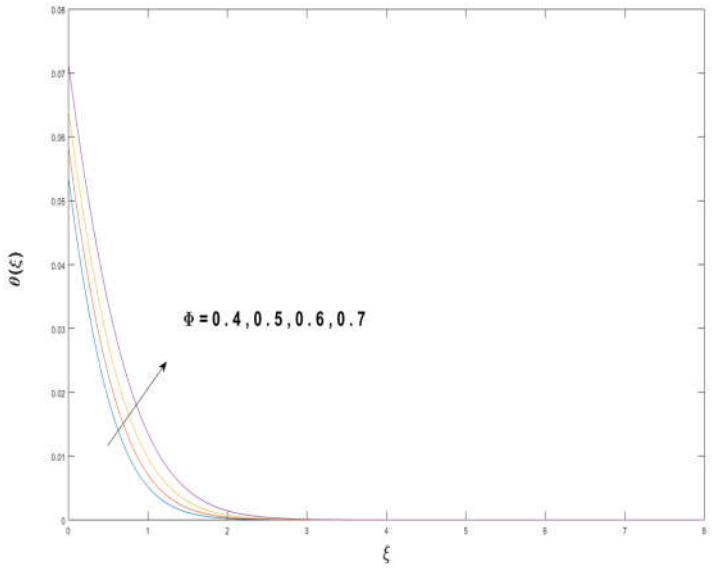

Figure 4.2: Effect of Φ on $\theta(\xi)$.

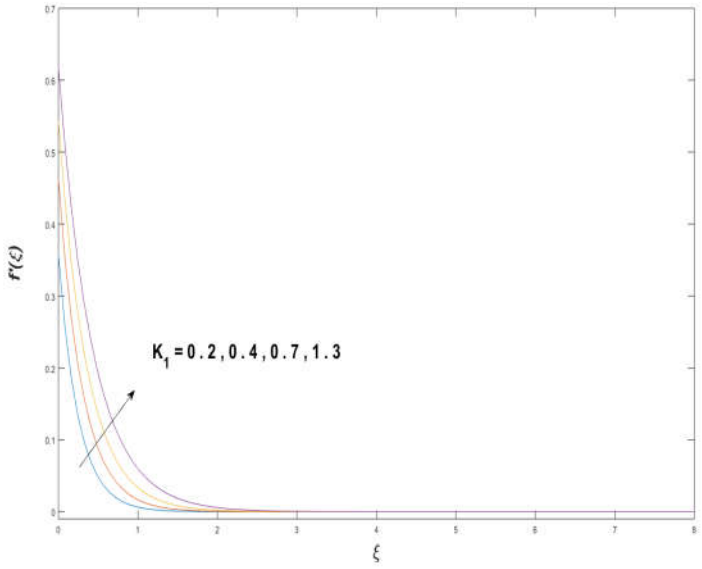

Figure 4.3: Effect of K_1on $f'(\xi)$.

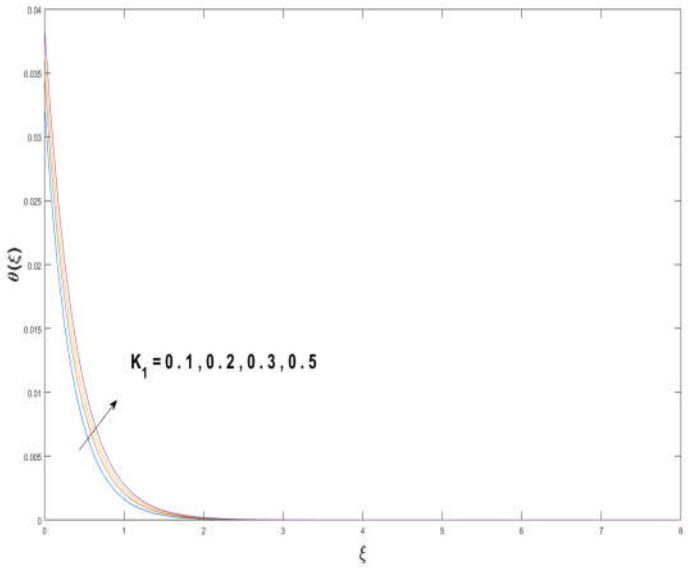

Figure 4.4: Effect of K_1 on $\theta(\xi)$.

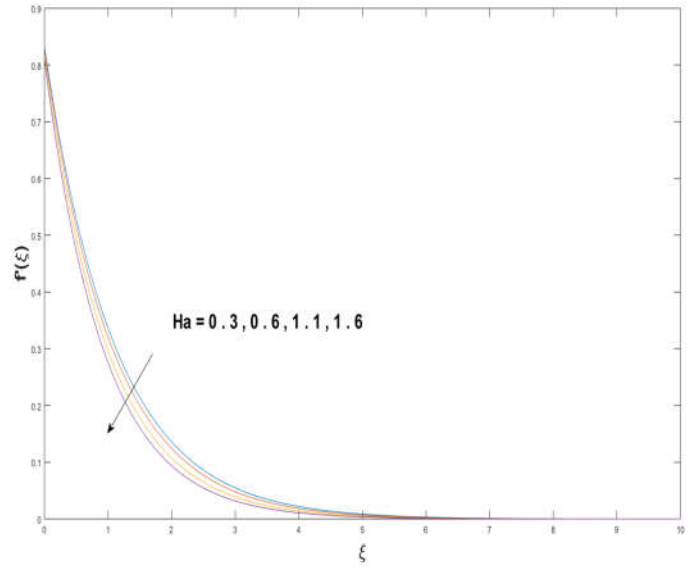

Figure 4.5: Effect of Ha on $f'(\xi)$.

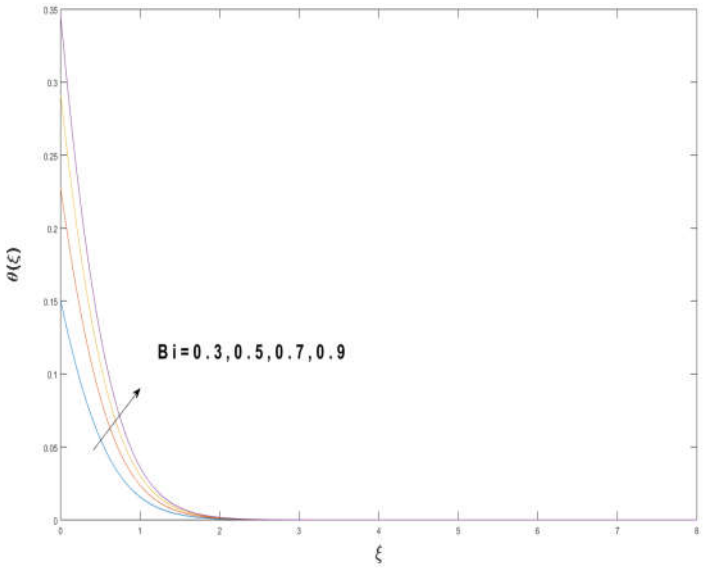

Figure 4.6. Effect of Bi on $\theta(\xi)$.

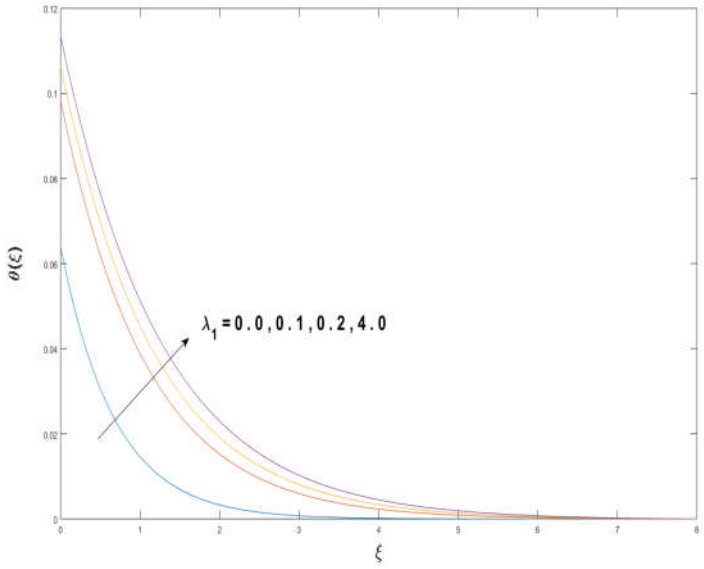

Figure 4.7. Effect of λ_1 on $\theta(\xi)$.

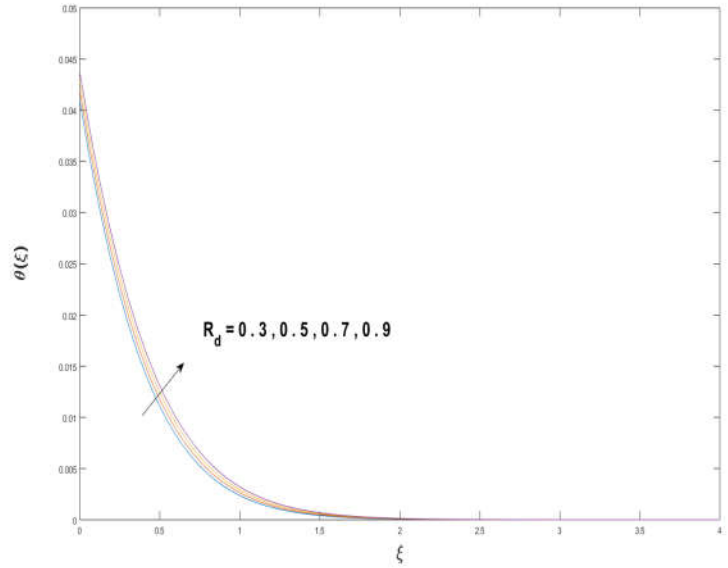

Figure 4.8. Effect of R_d on $\theta(\xi)$.

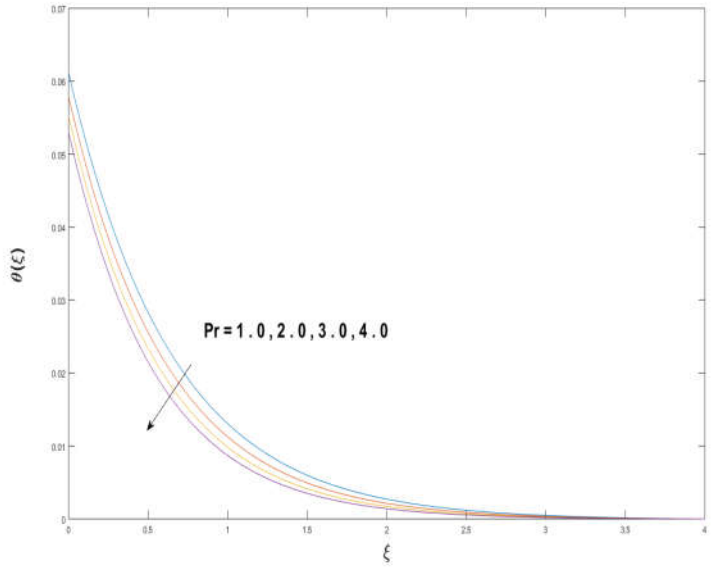

Figure 4.9. Effect of Pr on $\theta(\xi)$.

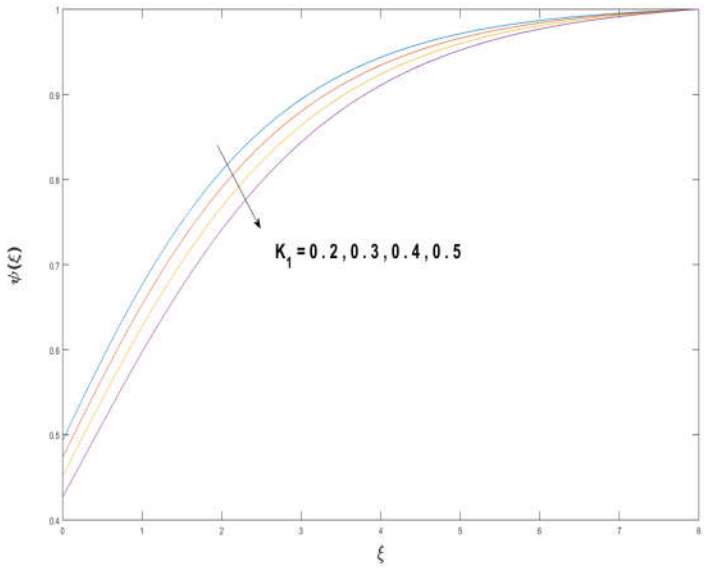

Figure 4.10. Effect of K_1 on $\psi(\xi)$.

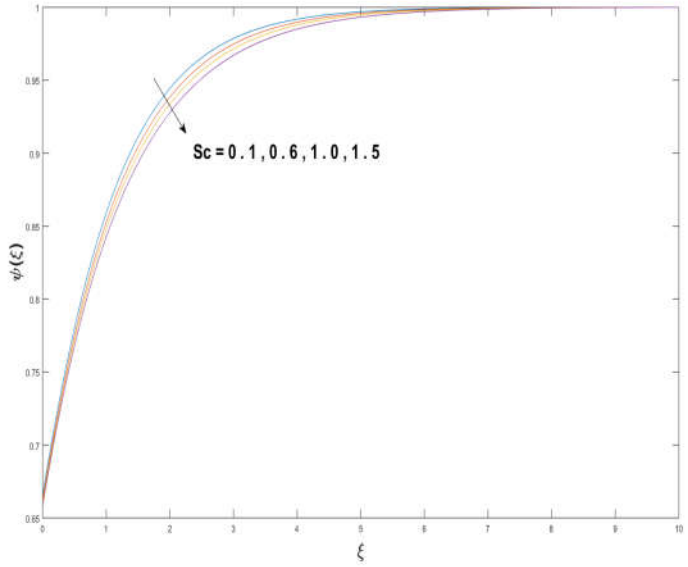

Figure 4.11. Effect of Sc on $\psi(\xi)$.

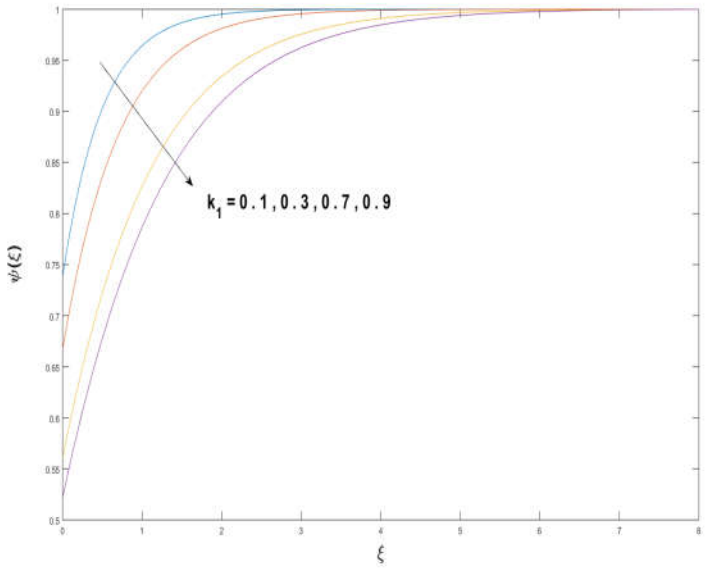

Figure 4.12. Effect of k_1 on $\psi(\xi)$.

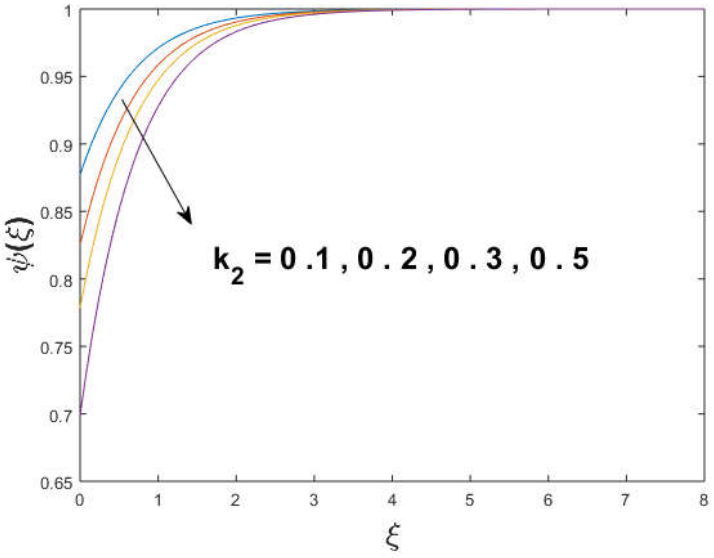

Figure 4.13. Effect of k_2 on $\psi(\xi)$.

Table 4.1: Values of Nusselt number $Nu(\mathrm{Re}_x)^{\frac{-1}{2}}$ and Skin fricition coefficient $-\frac{1}{2}C_f(\mathrm{Re}_x)^{\frac{1}{2}}$

K_1	Ha	Φ	Bi	R_d	λ_1	θ_w	$-\frac{1}{2}C_f(\mathrm{Re}_x)^{\frac{1}{2}}$	$Nu(\mathrm{Re}_x)^{\frac{-1}{2}}$
0.8	0.4	0.5		0.5	0.5	0.5	1.9567	0.3221
1.0							2.0963	0.3215
1.3							2.1979	0.3210
0.8	0.1						1.9369	0.3221
	0.3						1.9501	0.3221
	0.5						1.9633	0.3221
	0.1	0.02					0.3837	0.1013
		0.2					0.6297	0.1577
		0.5					1.9369	0.3221
		0.5	0.7				_	1.7136
			1.0				-	2.1923
			1.5				-	2.8072
			2.0	0.1			-	3.2456
				0.3			-	3.2582
				0.5			-	3.2706
				0.7	0.7		-	3.4474
					0.9		-	3.5804
					1.0		-	3.6385
					0.7	0.5	-	3.4474
						0.7	-	3.4319
						0.9	-	3.4075
						1.0	-	3.3918

Chapter 5

Conclusions and future work

In this thesis two problems have been analyzed where first problem is about review paper and second problem is the extension work of it. Conclusions of both the problems are as follows:

5.1 Chapter 3

- Increase in curvature parameter is correlaed with the reduction in concentration distribution and increase in velocity and temperature fields.
- Both profiles velocity and temperature show increasing behavior with increasing solid volume fraction.
- Temperature rises for higher values of Biot number.
- Increase in axil velocity field is seen under the influence of considerable magnetic parameter.
- The value of fraction factor profile increases for larger values of Ha and Φ, but opposit behavior in case of K_1 and Ha.
- Nusselt number reduces for higher values of $K_1$and R_d.

5.2 Chapter 4

- The velocity $f'(\xi)$ is an increasing function of solid volume fraction Φ.
- The velocity increases with decrease in Ha Hartmann number.
- For higher values of Biot number Bi, heat generation parameter λ_1, and for solid volume fraction ϕ temperature of the fluid boosted.
- The concentration distribution has opposite behavior for homogenous and heterogenous parameters k_1 and k_2.
- The concentration of the fluid has dwindled for larger values of Schmidt number S_c and Prandtl number Pr.
- The concentration profile enhanced for larger values of radiation parameter R_d.
- Increase in Surface Drag force $-\frac{1}{2}C_f(\mathrm{Re}_x)^{\frac{1}{2}}$ is associated with the increasing values of Bi and Ha.

5.3 Future work

In this work, the effects of homogenous heterogenous reactions and thermal radiation on 2D steady, incompressible nanofluid flow on a curved sheet have been analyzed. However, there remains a need to further build on the current work so as to bring improvement about the concerned discourse. Few interesting possible extensions that could be researched in future are as follows:

- Any non-Newtonian fluid along with appropriate boundary conditions.
- Bio-convective nanofluid with microorganisms.
- Boundary conditions also be changed to melting heat or second order slip.
- Flow over a curve surface with activation energy.

Bibliography

[1] Choi, S. U., & Eastman, J. A. (1995). Enhancing thermal conductivity of fluids with nanoparticles (No. ANL/MSD/CP-84938; CONF-951135-29). Argonne National Lab., IL (United States).

[2] Masuda, H., Ebata, A., & Teramae, K. (1993). Alteration of thermal conductivity and viscosity of liquid by dispersing ultra-fine particles. Dispersion of Al_2O_3, SiO_2 and TiO_2 ultra-fine particles..

[3] Lee, S., Choi, S. S., Li, S. A., & Eastman, J. A. (1999). Measuring thermal conductivity of fluids containing oxide nanoparticles. Journal of Heat transfer, 121(2), 280-289.

[4] Eastman, J. A., Choi, S. U. S., Li, S., Yu, W., & Thompson, L. J. (2001). Anomalously increased effective thermal conductivities of ethylene glycol-based nanofluids containing copper nanoparticles. Applied Physics Letters, 78(6), 718-720.

[5] Xuan, Y., Li, Q., & Hu, W. (2003). Aggregation structure and thermal conductivity of nanofluids. AIChE Journal, 49(4), 1038-1043.

[6] Sarkar, J., Ghosh, P., & Adil, A. (2015). A review on hybrid nanofluids: recent research, development and applications. Renewable and Sustainable Energy Reviews, 43, 164-177.

[7] Li, H., Ha, C. S., & Kim, I. (2009). Fabrication of Carbon Nanotube/SiO_2 and Carbon Nanotube/SiO_2/Ag Nanoparticles Hybrids by Using Plasma Treatment. Nanoscale research letters NRL.

[8] Madhesh, D., & Kalaiselvam, S. (2014). Experimental analysis of hybrid nanofluid as a coolant. Procedia Engineering, 97, 1667-1675.

[9] Suresh, S., Venkitaraj, K. P., Selvakumar, P., & Chandrasekar, M. (2011). Synthesis of Al_2O_3–Cu/water hybrid nanofluids using two step method and its thermo physical properties. Colloids and Surfaces A: Physicochemical and Engineering Aspects, 388(1-3), 41-48.

[10] Abbasi, S. M., Rashidi, A., Nemati, A., & Arzani, K. (2013). The effect of functionalisation method on the stability and the thermal conductivity of nanofluid hybrids of carbon nanotubes/gamma alumina. Ceramics International, 39(4), 3885-3891.

[11] Yu, W., & Xie, H. (2012). A review on nanofluids: preparation, stability mechanisms, and applications. Journal of Nanomaterials, 2012, 1.

[12] Murshed, S. M. S., Leong, K. C., & Yang, C. (2008). Investigations of thermal conductivity and viscosity of nanofluids. International Journal of Thermal Sciences, 47(5), 560-568.

[13] Eastman, J. A., Choi, S. U. S., Li, S., Yu, W., & Thompson, L. J. (2001). Anomalously increased effective thermal conductivities of ethylene glycol-based nanofluids containing copper nanoparticles. Applied Physics Letters, 78(6), 718-720.

[14] Choi, C., Yoo, H. S., & Oh, J. M. (2008). Preparation and heat transfer properties of nanoparticle-in-transformer oil dispersions as advanced energy-efficient coolants. Current Applied Physics, 8(6), 710-712..

[15] Botha, S. S., Ndungu, P., & Bladergroen, B. J. (2011). Physicochemical properties of oil-based nanofluids containing hybrid structures of silver nanoparticles supported on silica. Industrial & Engineering Chemistry Research, 50(6), 3071-3077.

[16] Sidik, N. A. C., Mohammed, H. A., Alawi, O. A., & Samion, S. (2014). A review on preparation methods and challenges of nanofluids. International Communications in Heat and Mass Transfer, 54, 115-125.

[17] Maxwell, J. C. (1954). Electricity and magnetism (Vol. 2). New York: Dover.

[18] Hamilton, R. L., & Crosser, O. K. (1962). Thermal conductivity of heterogeneous two-component systems. Industrial & Engineering Chemistry Fundamentals, 1(3), 187-191.

[19] Iijima, S. (1991). Helical microtubules of graphitic carbon. nature, 354(6348), 56.

[20] Xue, Q. Z. (2005). Model for thermal conductivity of carbon nanotube-based composites. Physica B: Condensed Matter, 368(1-4), 302-307.

[21] Murshed, S. S., De Castro, C. N., Lourenço, M. J. V., Lopes, M. L. M., & Santos, F. J. V. (2011). A review of boiling and convective heat transfer with nanofluids. Renewable and Sustainable Energy Reviews, 15(5), 2342-2354.

[22] Timofeeva, E. V., Routbort, J. L., & Singh, D. (2009). Particle shape effects on thermophysical properties of alumina nanofluids. Journal of Applied Physics, 106(1), 014304.

[23] Keblinski, P., Phillpot, S. R., Choi, S. U. S., & Eastman, J. A. (2002). Mechanisms of heat flow in suspensions of nano-sized particles (nanofluids). International Journal of Heat and Mass Transfer, 45(4), 855-863.

[24] Keblinski, P., Eastman, J. A., & Cahill, D. G. (2005). Nanofluids for thermal transport. Materials Today, 8(6), 36-44.

[25] Sarkar, J., Ghosh, P., & Adil, A. (2015). A review on hybrid nanofluids: recent research, development and applications. Renewable and Sustainable Energy Reviews, 43, 164-177.

[26] Pak, B. C., & Cho, Y. I. (1998). Hydrodynamic and heat transfer study of dispersed fluids with submicron metallic oxide particles. Experimental Heat Transfer an International Journal, 11(2), 151-170.

[27] Xuan, Y., & Li, Q. (2000). Heat transfer enhancement of nanofluids. International Journal of heat and fluid flow, 21(1), 58-64.

[28] Nine, M. J., Batmunkh, M., Kim, J. H., Chung, H. S., & Jeong, H. M. (2012). Investigation of Al_2O_3-MWCNTs hybrid dispersion in water and their thermal characterization. Journal of nanoscience and nanotechnology, 12(6), 4553-4559.

[29] Baghbanzadeh, M., Rashidi, A., Rashtchian, D., Lotfi, R., & Amrollahi, A. (2012). Synthesis of spherical silica/multiwall carbon nanotubes hybrid nanostructures and investigation of thermal conductivity of related nanofluids. Thermochimica Acta, 549, 87-94.

[30] Munkhbayar, B., Tanshen, M. R., Jeoun, J., Chung, H., & Jeong, H. (2013). Surfactant-free dispersion of silver nanoparticles into MWCNT-aqueous nanofluids prepared by one-step technique and their thermal characteristics. Ceramics International, 39(6), 6415-6425.

[31] Jana, S., Salehi-Khojin, A., & Zhong, W. H. (2007). Enhancement of fluid thermal conductivity by the addition of single and hybrid nano-additives. Thermochimica Acta, 462(1-2), 45-55.

[32] Sundar, L. S., Singh, M. K., Ramana, E. V., Singh, B., Grácio, J., & Sousa, A. C. (2014). Enhanced thermal conductivity and viscosity of nanodiamond-nickel nanocomposite nanofluids. Scientific Reports, 4, 4039.

[33] Sundar, L. S., Singh, M. K., & Sousa, A. C. (2014). Enhanced heat transfer and friction factor of MWCNT–Fe_3O_4/water hybrid nanofluids. International Communications in Heat and Mass Transfer, 52, 73-83.

[34] Sundar, L. S., Ramana, E. V., Graça, M. P. F., Singh, M. K., & Sousa, A. C. (2016). Nanodiamond-Fe_3O_4 nanofluids: preparation and measurement of viscosity, electrical and thermal conductivities. International Communications in Heat and Mass Transfer, 73, 62-74.

[35] Naughton, B. T., & Clarke, D. R. (2007). Lattice expansion and saturation magnetization of nickel–zinc ferrite nanoparticles prepared by aqueous precipitation. Journal of the American Ceramic Society, 90(11), 3541-3546.

[36] Virden, A. E., & O'Grady, K. (2005). Structure and magnetic properties of NiZn ferrite nanoparticles. Journal of magnetism and magnetic materials, 290, 868-870..

[37] Shahane, G. S., Kumar, A., Arora, M., Pant, R. P., & Lal, K. (2010). Synthesis and characterization of Ni–Zn ferrite nanoparticles. Journal of Magnetism and Magnetic Materials, 322(8), 1015-1019.

[38] Sheikholeslami, M., Ganji, D. D., & Rashidi, M. M. (2015). Ferrofluid flow and heat transfer in a semi annulus enclosure in the presence of magnetic source considering thermal radiation. Journal of the Taiwan Institute of Chemical Engineers, 47, 6-17.

[39] Sheikholeslami, M., Ganji, D. D., & Rashidi, M. M. (2015). Ferrofluid flow and heat transfer in a semi annulus enclosure in the presence of magnetic source considering thermal radiation. Journal of the Taiwan Institute of Chemical Engineers, 47, 6-17.

[40] Neuringer, J. L. (1966). Some viscous flows of a saturated ferro-fluid under the combined influence of thermal and magnetic field gradients. International Journal of Non-Linear Mechanics, 1(2), 123-137.

[41] Majeed, A., Zeeshan, A., & Ellahi, R. (2016). Unsteady ferromagnetic liquid flow and heat transfer analysis over a stretching sheet with the effect of dipole and prescribed heat flux. Journal of Molecular Liquids, 223, 528-533.

[42] Crane, L. J. (1970). Flow past a stretching plate. Zeitschrift für angewandte Mathematik und Physik ZAMP, 21(4), 645-647.

[43] Gupta, P. S., & Gupta, A. S. (1977). Heat and mass transfer on a stretching sheet with suction or blowing. The Canadian Journal of Chemical Engineering, 55(6), 744-746.

[44] Chakrabarti, A., & Gupta, A. S. (1979). Hydromagnetic flow and heat transfer over a stretching sheet. Quarterly of Applied Mathematics, 37(1), 73-78.

[45] Andersson, H. I., Bech, K. H., & Dandapat, B. S. (1992). Magnetohydrodynamic flow of a power-law fluid over a stretching sheet. International Journal of Non-Linear Mechanics, 27(6), 929-936.

[46] Hayat, T., Muhammad, T., Shehzad, S. A., & Alsaedi, A. (2017). An analytical solution for magnetohydrodynamic Oldroyd-B nanofluid flow induced by a stretching sheet with heat generation/absorption. International Journal of Thermal Sciences, 111, 274-288.

[47] Sajid, M., Ali, N., Javed, T., & Abbas, Z. (2010). Stretching a curved surface in a viscous fluid. Chinese Physics Letters, 27(2), 024703.

[48] Muhammad, N., Nadeem, S., & Haq, R. U. (2017). Heat transport phenomenon in the ferromagnetic fluid over a stretching sheet with thermal stratification. Results in Physics, 7, 854-861.

[49] Ramzan, M., & Yousaf, F. (2015). Boundary layer flow of three-dimensional viscoelastic nanofluid past a bi-directional stretching sheet with Newtonian heating. AIP Advances, 5(5), 057132.

[50] Sanni, K. M., Asghar, S., Jalil, M., & Okechi, N. F. (2017). Flow of viscous fluid along a nonlinearly stretching curved surface. Results in Physics, 7, 1-4.

[51] Hussain, T., Shehzad, S. A., Hayat, T., Alsaedi, A., Al-Solamy, F., & Ramzan, M. (2014). Radiative hydromagnetic flow of Jeffrey nanofluid by an exponentially stretching sheet. Plos One, 9(8), e103719.

[52] Goto, Y., Kamebuchi, Y., Hagio, T., Kamimoto, Y., Ichino, R., & Bessho, T. (2018). Electrodeposition of copper/carbonous nanomaterial composite coatings for heat-dissipation materials. Coatings, 8(1), 5.

[53] Park, J. E., Jang, Y. S., Bae, T. S., & Lee, M. H. (2018). Multi-Walled carbon nanotube coating on alkali treated TiO_2 nanotubes surface for improvement of bio-compatibility. Coatings, 8(5), 159..

[54] Rivero, P. J., Garcia, J. A., Quintana, I., & Rodriguez, R. (2018). Design of nanos-tructured functional coatings by using wet-chemistry methods. Coatings, 8(2), 76.

[55] Ramzan, M., Bilal, M., Chung, J. D., Lu, D. C., & Farooq, U. (2017). Impact of generalized Fourier's and Fick's laws on MHD 3D second grade nanofluid flow with variable thermal conductivity and convective heat and mass conditions. Physics of Fluids, 29(9), 093102.

[56] Merkin, J. H. (1996). A model for isothermal homogeneous-heterogeneous reactions in boundary-layer flow. Mathematical and Computer Modelling, 24(8), 125-136.

[57] Chaudhary, M. A., & Merkin, J. H. (1995). A simple isothermal model for homogeneous-heterogeneous reactions in boundary-layer flow. I Equal Diffusivities. Fluid Dynamics Research, 16(6), 311.

[58] Bachok, N., Ishak, A., & Pop, I. (2011). On the stagnation-point flow towards a stretching sheet with homogeneous–heterogeneous reactions effects. Communications in Nonlinear Science and Numerical Simulation, 16(11), 4296-4302.

[59] Khan, W. A., & Pop, I. M. (2012). Effects of homogeneous–heterogeneous reactions on the viscoelastic fluid toward a stretching sheet. Journal of Heat Transfer, 134(6), 064506.

[60] Shaw, S., Kameswaran, P. K., & Sibanda, P. (2013). Homogeneous-heterogeneous reactions in micropolar fluid flow from a permeable stretching or shrinking sheet in a porous medium. Boundary Value Problems, 2013(1), 77.

[61] Kameswaran, P. K., Shaw, S., Sibanda, P. V. S. N., & Murthy, P. V. S. N. (2013). Homogeneous–heterogeneous reactions in a nanofluid flow due to a porous stretching sheet. International Journal of Heat and Mass Transfer, 57(2), 465-472.

[62] Hayat, T., Imtiaz, M., Alsaedi, A., & Almezal, S. (2016). On Cattaneo–Christov heat flux in MHD flow of Oldroyd-B fluid with homogeneous–heterogeneous reactions. Journal of Magnetism and Magnetic Materials, 401, 296-303.

abida

ORIGINALITY REPORT

16%	8%	11%	8%
SIMILARITY INDEX	INTERNET SOURCES	PUBLICATIONS	STUDENT PAPERS

PRIMARY SOURCES

1	www.mdpi.com Internet Source	3%
2	Submitted to Higher Education Commission Pakistan Student Paper	2%
3	journals.plos.org Internet Source	1%
4	Submitted to Athlone Institute of Technology Student Paper	<1%
5	www.worldscientific.com Internet Source	<1%
6	Imtiaz, Maria, Tasawar Hayat, Ahmed Alsaedi, and Aatef Hobiny. "Homogeneous-heterogeneous reactions in MHD flow due to an unsteady curved stretching surface", Journal of Molecular Liquids, 2016. Publication	<1%
7	Behrouz Takabi, Hossein Shokouhmand. " Effects of – /water hybrid nanofluid on heat	<1%